COUNTER CURRENT FLOW PHENOMENON AND PRESSURE DROP CALCULATION IN ANNULAR GEOMETRY

A THESIS SUBMITTED IN PARTIAL FULFILLMENT OF
THE REQUIREMENTS FOR THE DEGREE OF

MASTER OF TECHNOLOGY

In

MECHANICAL ENGINEERING

[Specialization: Thermal Engineering]

By

CHANDRANAN KUMAR
Roll No. 207ME303

Department of Mechanical Engineering
National Institute of Technology
Rourkela
May, 2009

COUNTER CURRENT FLOW PHENOMENON AND PRESSURE DROP CALCULATION IN ANNULAR GEOMETRY

A THESIS SUBMITTED IN PARTIAL FULFILLMENT OF
THE REQUIREMENTS FOR THE DEGREE OF

MASTER OF TECHNOLOGY

In

MECHANICAL ENGINEERING

[Specialization: Thermal Engineering]

By

CHANDRANAN KUMAR
Roll No. 207ME303

Under the supervision of

Dr. S. K. SAHU

Department of Mechanical Engineering
National Institute of Technology
Rourkela
May, 2009

National Institute of Technology

Rourkela

CERTIFICATE

This is to certify that the work in this thesis entitled **"COUNTER CURRENT FLOW PHENOMENON AND PRESSURE DROP CALCULATION IN ANNULAR GEOMETRY"** by **CHANDRANAN KUMAR** has been carried out under my supervision in partial fulfillment of the requirements for the degree of **"Master of Technology"** in **Mechanical Engineering** with specialization in **"Thermal Engineering"** during session 2008 - 2009 in the Department of Mechanical Engineering, National Institute of Technology, Rourkela.

To the best of my knowledge, the matter incorporated in this thesis has not been submitted to any other University/Institute for the award of any degree or diploma.

Date: 26.05.09.

Place: NIT Rourkela.

Dr. S. K. SAHU
Department of Mechanical Engineering
National Institute of Technology
Rourkela - 769008

ACKNOWLEDGEMENT

Setting an endeavour may not always be an easy task; obstacles are bound to come in this way & when this happens, help is welcome & needless to say without help of the those people whom I am going to address here, this endeavour could not have been successful & I owe my deep sense of gratitude & warm regards to my supervisor **DR. S. K. SAHU, Dept of Mechanical Engineering, NIT Rourkela** for suggesting me an exhaustive & challenging topic pertaining to my dissertation work as well as his able monitoring throughout the course of my work. I am greatly indebted to him for his constructive suggestions and selfless help perennially during the course of progress of my work. Thank you, Sir.

I extend my thanks to **Dr. R. K. SAHOO, Professor and Head, Dept. of Mechanical Engineering** for extending all possible help in carrying out the dissertation work directly or indirectly.

I greatly appreciate & convey my heartfelt thanks to my colleagues' flow of ideas, dear ones & all those who helped me in completion of this work.

This acknowledgement would be incomplete without **Mr. S. K. Nanda**, Research Scholar, Dept. of Mining Engineering, NIT Rourkela for his endless support and remarkable suggestions. Thank you, Sir, for being with me in times of need and pulling my cart out of trouble.

Special thanks to my parents & elders without their blessings & moral enrichment I could not have landed with this outcome.

Above all, even though, he does not need any credit, but my prayers & ovations to the Omnipotent**,** who strengthened me to stand with smile against the odds coming in this course of work without fail & blessed me with this fruit of work for my dedication.

NIT Rourkela **CHANDRANAN KUMAR**

ABSTRACT

Liquid films falling under the influence of gravity are widely encountered in a variety of industrial two-phase flow applications (distillation columns, nuclear reactor cores, wetted walls and packed towers, heat pipes, vertical condensers etc.). The falling annular film represents a fundamental limiting case of the annular flow regime of two-phase gas-liquid flows. The maximum flow rates of gas and liquid phases which flow in opposite-directions (counter-current flow) are limited by a phenomenon known as a Counter-Current Flow Limitation (CCFL or flooding). In other words, flooding phenomenon is defined as the transition of part of liquid to a climbing film on increasing gas velocity. Flooding makes the limit of stable counter current flow.

The calculation of pressure drop in nuclear fuel bundles across its different components is very complex and is not discussed vastly in the literature. In general, spacers of various configurations like wire wrapped, honey comb, grid type are used in the fuel rod bundles to provide support to the fuel pins as well as facilitates in effective cooling of the fuel pins, but the pressure drop across it is appreciable.

This dissertation investigates the film thickness model in gas liquid two phase annular flow as well as pressure drop estimation in annular geometry such as fuel bundles and spacers. A mathematical model for the estimation of film thickness has been derived by the application of fundamental momentum equation and a numerical iterative technique with programming in MatLab has been done to estimate the film thickness in falling film, a limiting case of gas liquid annular flow. An experimental test facility has been proposed to study and visualize the gas liquid interactions, flooding phenomenon and measurement of film thickness.

Spacer loss coefficient and subsequently, pressure drop in D5 fuel cluster have been estimated with the help of developed correlations based on flow area ratio. As this flow area ratio increases the spacer loss coefficient decrease & vice-versa for a given length of the spacer, but it increases with increase in the spacer length.

Pressure drop across spacer is noticeable and amounts to an appreciable percentage of the total pressure drop in the fuel cluster.

Keywords: Gas-liquid flow, CCFL, Flow Regimes, Annular flow, Falling Films, Rod Bundles, Spacer, and Pressure Drop.

CONTENTS

CERTIFICATE iii

ACKNOWLEDGEMENT iv

ABSTRACT v

CONTENTS vii

NOMENCLATURE ix

LIST OF FIGURES xii

LIST OF TABLES xiv

CHAPTER 1 INTRODUCTION

1.1 Background 1

1.1.1 Flow patterns in vertical gas-liquid two phase flows 1

1.1.2 Annular Flow 3

1.1.3 Interfacial Waves 3

1.2 Counter Current Flow Phenomenon 5

1.3 Pressure Drop: Rod Bundle & Spacers 7

1.3.1 Components of Pressure Drop 9

1.3.2 Spacers 10

1.4 Objective & Organization of thesis 13

CHAPTER 2 LITERATURE REVIEW

2.1 Theoretical Models & Correlations 14

2.2 Flooding Mechanisms 21

2.2.1 Kinematic Waves 21

2.2.2 Upward Liquid Film Flow 23

2.2.3 Drop Entrainment 23

2.3 Geometrical Dependencies 24

2.4 Pressure Drop: Rod Bundle & Spacers 26

2.5 D5 Fuel Cluster 28

CHAPTER 3 ANALYTICAL STUDY

3.1 Flooding Condition 31

3.2 Film Thickness Model in Annulus 35

3.3 Pressure Loss Coefficient at Spacer 39

3.4 Pressure Drop Calculation in D5 Fuel Cluster 42

CHAPTER 4 EXPERIMENTAL DESIGN

4.1 Structure 48

4.2 Acrylic Components 49

4.2.1 The Air Outlet 49

4.2.2 Upper Plenum 50

4.2.3 Test Section 51

4.2.4 Lower Plenum 52

4.3 Instrumentation 53

4.3.1 Instruments & Equipments 53

4.3.2 Data Acquisition System 55

CHAPTER 5 RESULTS & DISCUSSION

5.1 Film Thickness Model Validation 56

5.2 Spacer Loss Coefficient Discussion 58

5.3 Pressure Drop Verification 61

CHAPTER 6 CONCLUSION & FUTURE WORK 63

REFERENCES 64

APPENDIX A 69

APPENDIX B 70

NOMENCLATURE

Q_G	Generated power within the core
Q_E	Extracted power
W	Mass flow rate (Kg/sec)
ΔI	Enthalpy difference between the core outlet and inlet
ΔP_f	Pressure drop due to skin friction
ΔP_l	Pressure drop due to form friction (local friction drop)
ΔPe	Elevation pressure drop.
ΔP_a	Acceleration pressure drop
D_h	Hydraulic diameter (mm)
K	Local loss coefficient
A_0	Smaller flow area (m^2)
Ar	Area ratio
V_L^*	Liquid dimensionless superficial velocity
V_G^*	Gas dimensionless superficial velocity
g	Acceleration due to gravity (m/s^2)
ρ	Density of the fluid (Kg/m^3)
Ku	Kutateladze number
C_w	Wall friction factor
N'_B	Bond number
S	Ratio of gap size to average circumference
Bo	Bond number
Fr	Froude number
μ	Dynamic viscosity ($N\text{-}s/m^2$)
$\bar{\alpha}$	Average gas volume fraction
J_f	Liquid volumetric flux (m/s)

Jg	Gas volumetric flux (m/s)
We_c	Weber Number
C_d	Drag coefficient of the drop
D^*	Dimensionless diameter
A	Cross sectional areas
U	Mean velocity (Kg/sec)
Δp	Pressure loss
$\frac{A_{G1}}{A_{G0}}$	Ratio of area at the open section to area at the lump
Δh	Height the lump of large wave (mm)
δ_w	Width of the lump of large wave (mm)
D	Rod/fuel pin diameter (mm)
τ_w	Shear stress on the rod surface
r, z	Cylindrical coordinates
u	Velocity of falling liquid film (m/sec)
δ_{cc}	Film thickness in counter current flow situation (mm)
δ_{ff}	Free falling film thickness in the absence of air (mm)
Q	Flow rate of falling film
ΔP_{SP}	Spacer pressure loss
ΔP_C	Contraction pressure loss
ΔP_E	Expansion pressure loss
V	Coolant velocity (m/sec)
L	Length of a spacer (mm)
f	Friction loss coefficient
ζ_C	Coefficient of the pressure loss due to the contraction
ζ_E	Coefficient of the pressure loss due to the expansion
De	Equivalent hydraulic diameter of rod bundle (mm)
n	Number of fuel rods
N	Number of spacers

$\left(\frac{A_2}{A_1}\right)$	Flow area ratio/blockage ratio (m^2)
Di	Shroud diameter (mm)
Dcr	Coolant tube diameter (mm)
Ds	Spacer diameter (mm)
D_h	Fuel pin hole outer diameter (mm)
D_{hi}	Fuel pin hole inner diameter (mm)
D_{ho}	Fuel pin hole outer diameter (mm)
Δz	Height of fuel assembly (m)
Re	Reynolds Number.

Subscripts & Abbreviations

sp	Spacer
cc	Counter current situation
ff	Free falling film
G	Gas
L	Liquid
CCFL	Counter current flow phenomenon.
LOCA	Loss of Coolant Accident
ECCS	Emergency core cooling system
AHWR	Advanced Heavy Water Reactor
PWR	Pressurised Water Reactor
cr	Coolant rod
i	Shroud

LIST OF FIGURES

FIGURE		PAGE
1.1	Flow pattern in vertical two-phase flow regimes.	2
1.2	Schematic of two phase annular flow.	3
1.3	Disturbance & ripple waves.	4
1.4	Schematic of counter current flow phenomenon in concentric tubes.	5
1.5	Flow transition from counter current flow to concurrent up flow in vertical tube.	6
1.6	Countercurrent flow of steam & cooling water in hot leg of PWR during loss of coolant accident.	7
1.7	Various spacer grids.	11
1.8	Commonly used spacer grids.	12
2.1	Flow pattern map for vertical counter current pipe 5cm in diameter.	18
2.2	Graphical Solution to drift flux problem.	22
2.3	Geometries of tube ends used for air & liquid exit & entry.	24
2.4	Arrangement of 54 pin cluster.	29
2.5	AHWR D5 cluster details.	30
3.1	Analytical model for flooding in annular geometry.	32
3.2	Falling film in circular tubular geometry.	35
3.3	Flow chart for calculation of film thickness.	38
3.4	Schematic of pressure loss components at spacer.	40
3.5	Simulated D5 fuel cluster.	43
3.6	Symmetrical distribution of fuel pins at spacer cross section.	43
3.7	Flow chart for the pressure drop calculation in D5 fuel cluster.	45
4.1	Schematic of proposed experimental set up.	47

4.2	Schematic of test section showing the relative locations of the fluid inlets & outlets.	50
4.3	Schematic of water entry in the upper plenum of test section.	51
4.4	Schematic of air inlet & liquid outlet.	52
4.5	Magnetic flow meter.	54
5.1	Plot of flow rate vs. film thickness.	58
5.2	Plot of loss coefficient vs. area ratio for changing length of spacer.	59
5.3	Plot of bundle friction factor vs. Reynolds number.	61
5.4	Plot of pressure drop in a D5 fuel cluster vs. coolant velocity.	61
5.5	Plot of individual pressure drop in a D5 fuel cluster.	62

LIST OF TABLES

TABLE		PAGE
1.1	Factors affecting the pressure drop in rod bundles.	8
3.1	Spacer & fuel pin dimensions & coolant property.	44
4.1	Properties of fluids to be used in the proposed set up.	48
4.2	Experimental measurements & devices.	53
5.1	Comparison of theoretical & standard values of film thickness.	57
5.2	Comparison of spacer loss coefficient for varying spacer length & area ratio.	59
5.3	Bundle friction factor at different Reynolds number.	60
5.4	Component of individual pressure drops in D5 fuel cluster.	62

CHAPTER 1

INTRODUCTION

BACKGROUND

COUNTER CURRENT FLOW PHENOMENON

PRESSURE DROP: ROD BUNDLES & SPACERS

OBJECTIVE & ORGANISATION OF THESIS

INTRODUCTION

Gas-liquid annular flow is an important two-phase flow regime. In case of two-phase flow, there exists several important and as of yet still unclarified phenomena. These phenomena affect many aspects of engineering design from calculations of pressure drops to the analysis of heat transfer characteristics. One such phenomena is known as the counter current flow limitation, or CCFL, and its appearances are many, its effects, legion. It frequently occurs in thermal management and thermal control systems in terrestrial and non terrestrial energy transport systems such as nuclear reactors, power plants, boilers, heat pipes, wetted walls and packed tower in heat exchangers, and space stations. In order to design these systems with greater efficiency and lower cost, a basic understanding of the physical processes occurring in falling films is needed. Free falling films under the influence of gravity are the limiting case of gas liquid two phase flows. It is very important to be able to predict the factors behind such phenomenon to avoid its actual occurrence, particularly in situations where the effects could be quite disastrous. However, the onset of the entrainment process and its progress through the formation of "disturbance waves" responsible for the phenomenon is poorly understood. Free falling films under the influence of gravity are the limiting case of gas liquid two phase flows.

1.1 BACKGROUND

In this section, the basic flow patterns observed in vertical gas-liquid two-phase flows has been briefly discussed. Following this, the special case of falling annular films, a limiting case of two phase gas liquid flow is introduced as well as the concept of interfacial waves and their classifications originating due to the interaction of liquid and gas medium at their common surface and its dependency on geometry has been also been discussed.

1.1.1 FLOW PATTERNS IN VERTICAL GAS-LIQUID TWO PHASE FLOW

A flow regime is a geometrical configuration taken up by the gas and liquid in a two phase flow. For conditions of technological interest, there are a few major types of flow regimes observed for gas-liquid flow in pipes. Characteristics of these flow regimes, and the conditions under which these flow patterns exist, depend on (among other things) the orientation of the pipe with respect to gravity. Figure 1.1 shows the flow patterns that are observed in vertical downward gas-liquid flows.

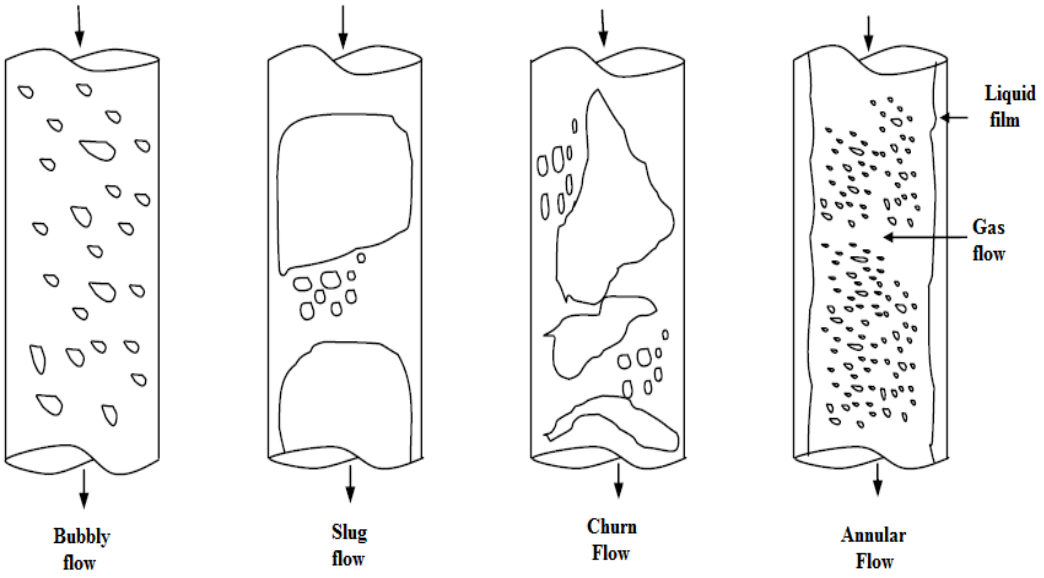

Fig. 1.1: Flow pattern in vertical two-phase flow regimes [1].

At low gas flow rates a bubbly flow pattern, in which small gas bubbles spherical or nearly spherical in nature are uniformly distributed in the liquid is obtained. Increasing the gas flow rate leads to slug flow. This flow pattern is characterised by large bullet-shaped gas bubbles separated by liquid slugs filling the entire cross section of the tube. At even higher gas flow rates, a highly agitated churn flow is observed. It could be viewed as a transition between slug and annular flows. This flow regime is usually very small or absent in vertical downward flows. Increasing the gas flow rate further leads to the annular flow regime in which the liquid moves along the pipe wall as a thin, wavy film and the gas flows in the core region as shown in figure 1.1. Here, most of the liquid is present in the film and the liquid film may or may not contain gas bubbles. Also, the gas core may or may not contain entrained liquid droplets. This flow pattern is very important in two-phase heat transfer applications because it immediately precedes the "dry out condition" where there is breakdown of the liquid film on the wall.

The falling annular film represents a fundamental limiting case of the annular flow regime of two-phase gas-liquid flows. The liquid film descends on the walls and there is no net flow of gas in the pipe. This means that the gas core is a constant pressure region. As for other flows, falling films can be broadly classified into laminar and turbulent film flows. The most important flow, which is of greater practical interest, is the turbulent film flow where there are random fluctuations in the velocity field. The flow is more complicated due to the presence of waves on the gas-liquid interface and is

considered to be unsteady and non-uniform. The presence of waves enhances the macroscopic transport properties of the system.

1.1.2 ANNULAR FLOW

In vertical upward gas-liquid two-phase flow, with increasing the gas flow rate, the flow usually changes from bubbly flow to slug flow (or plug flow) to churn flow and finally to annular flow. Annular two-phase flow is the focus of this work. It is characterized by a gas core flowing in the centre of the tube, a liquid film flowing on the inner tube wall, and a gas-liquid interface covered with waves. The gas core also carries entrained liquid droplets. The droplets are believed to be transported into the gas core as crests of the waves are sheared off by the gas stream. Fig.1.2 below is a schematic of a typical two-phase annular flow regime.

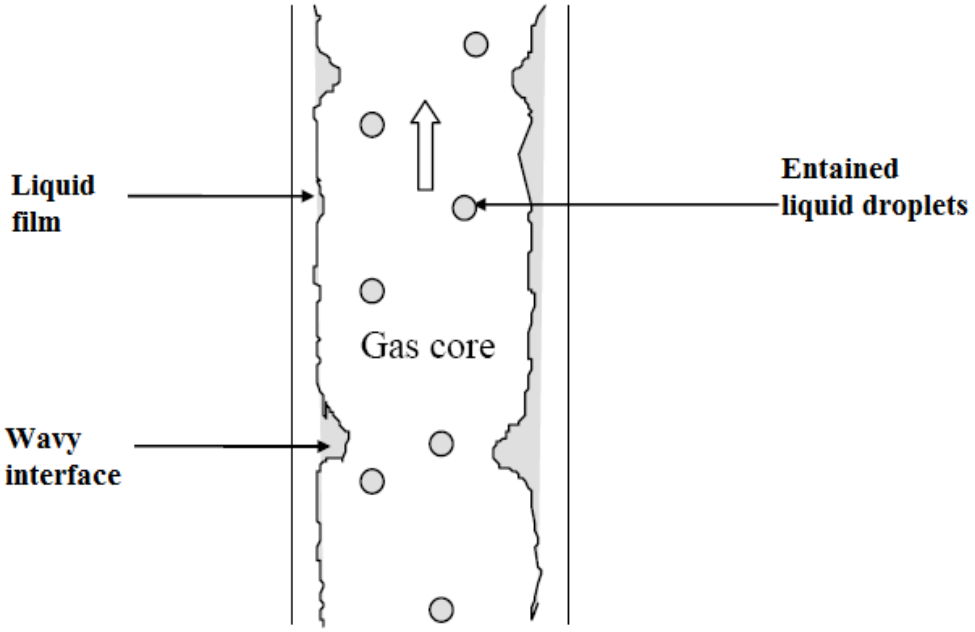

Fig. 1.2: Schematic of two-phase annular flow [2].

1.1.3 INTERFACIAL WAVES

A significant feature of annular flow is the presence of waves with various scales on the two-phase interface. While the two-phase flow literature contains many types and names for interfacial waves, there is agreement that two types are typically present. They are called “ripple waves” and “disturbance waves”. Ripple waves have small amplitudes compared with the liquid film thickness. Their wavelengths are usually measured in several millimetres. Their life time is short and they usually do not occupy the whole

tube circumference. Disturbance waves are sometimes called “roll waves”. They have a longer lifespan, and their amplitudes are usually several times the liquid film thickness. Their wavelengths are several tube diameters for flow in a small-diameter tube. In addition, for annular flow in a small-diameter tube (Tube ID < 58 mm), the liquid film is uniformly distributed around the tube circumference, and disturbance waves appear circumferentially coherent, two-dimensional, and circumferentially symmetrical. These characteristics of disturbance waves are obviously important in modelling of waves and the flow phenomena associated with them. A disturbance wave has a steep front and a long region of relatively quiet fluid between crests (Fig.1.3). Several investigations on the disturbance wave configurations were performed in the past.

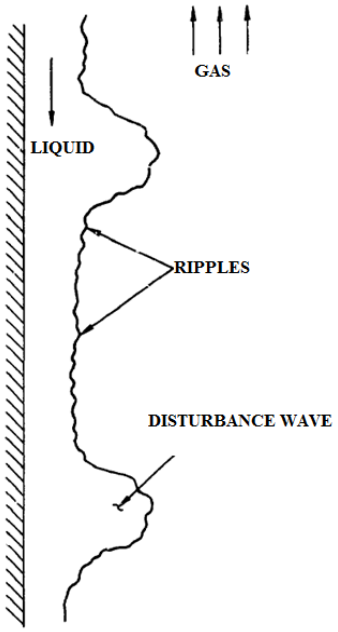

Fig. 1.3: Disturbance and Ripple waves [3].

At very low liquid flow rates the ripple waves dominate the two-phase interface. The surface looks smooth and appears to be laminar between waves. Above a critical liquid flow rate, disturbance waves appear in the flow and exert strong influence on the flow due to their significant dimensions and dynamic properties. Unlike disturbance waves, ripple waves exist over the full range of annular flow. Due to their minor role, ripple waves are usually not considered. Waves play crucial roles in the transport processes in annular flow such as mass transfer, momentum transfer, and heat transfer between the phases. Waves are mentioned here because they significantly contribute to the liquid entrainment phenomena and mechanisms in annular flows.

1.2 COUNTER CURRENT FLOW PHENOMENON

Counter current flow is defined as the two-phase flow regime in which the working fluids of a system flow with velocities of opposite signs; that is, fluids flowing in opposite directions (Fig 1.4). A simplified example of such a flow would be the downward flow of milk leaving a bottle with the upwards flow of air replacing the subsequent void. As the liquid leaves the bottle, the remaining volume must be replaced by some fluid, in this case air. Thus, there exists a counter current flow situation in which milk is flowing with the aid of gravity into a pint glass and air is flowing in the opposite direction due to a pressure difference. Furthermore, if the milk is poured too quickly, a violent and chaotic situation arises: flooding. If the rate at which the liquid leaves the vessel is great enough that the associated air owing into the vessel inhibits the flow of both, CCFL is said to have been achieved.

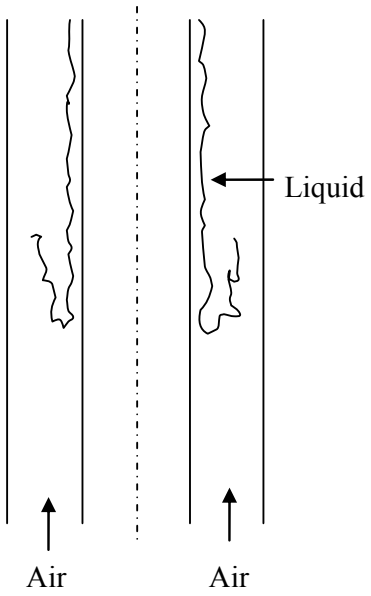

Fig 1.4: Schematic of Counter current flow phenomenon in concentric tubes.

It is also necessary to introduce the term “flooding”. In the literatures surveyed so far, the term flooding is synonymous with CCFL. While CCFL and flooding both refer to essentially the same phenomenon, CCFL is defined as the point at which the relative velocities of two fluids results in a change in the direction of a portion of the liquid phase. The key word in the definition is point; that is, an instant when the phenomenon occurs which is different than the continuous nature of “flooding”. Flooding is the

situation associated with the system when at least a measurable portion of the liquid phase is flowing in the direction of the gaseous phase. Put another way, CCFL can be described as the onset of flooding, but not as the phenomenon of flooding itself. This thesis deals with CCFL, the onset of flooding, and not the characteristics of a system during the flooding stage.

In other words, flooding phenomenon is defined as the transition of part of liquid to a climbing film on increasing gas velocity. Flooding makes the limit of stable counter current flow. Any further increase in either the gas flow rate or the liquid flow rate would destabilize the counter current flow to form concurrent flow above the inlet point. At each particular gas flow rate there is a maximum liquid flow rate and vice versa (Fig.1.5). The gas phase velocity that makes CCFL occur is called CCFL gas velocity or flooding gas velocity. With less flow rate than CCFL liquid velocity, all the water supplied to a liquid entrance penetrates the flow path. However, most of supplied liquid accumulates above the liquid entrance if flooding occurs.

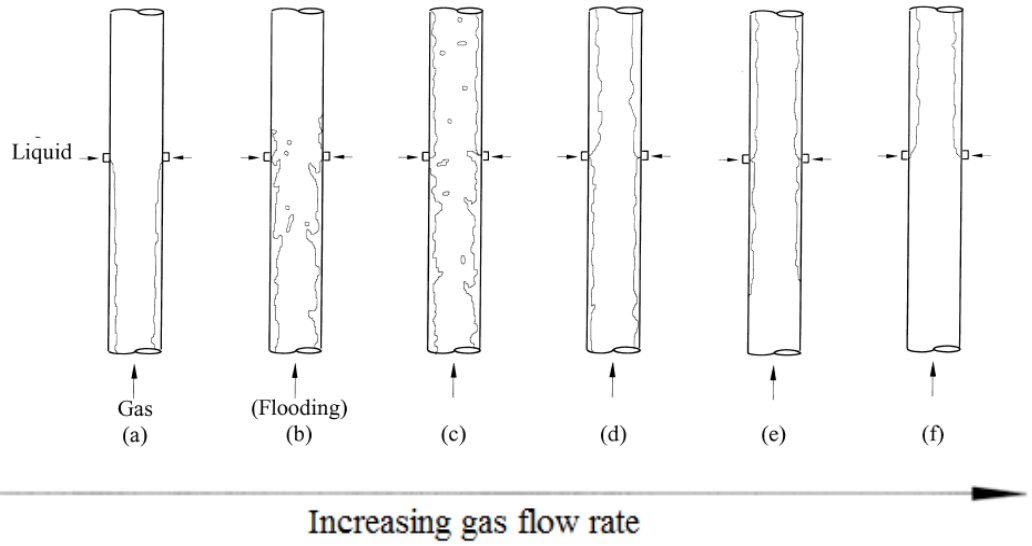

Fig.1.5: Flow transitions from counter current flow to concurrent up flow in vertical tube [4].

CCFL affects a great variety of systems both within the nuclear industry and beyond such as

1) Design criterion in various process equipments such as evaporators, heat pipes, and compact heat exchangers.
2) Wetted walls & packed towers in chemical engineering.

3) In Emergency Core Cooling System (ECCS) of nuclear reactors during Loss of Coolant Accident (LOCA) (Fig1.6).

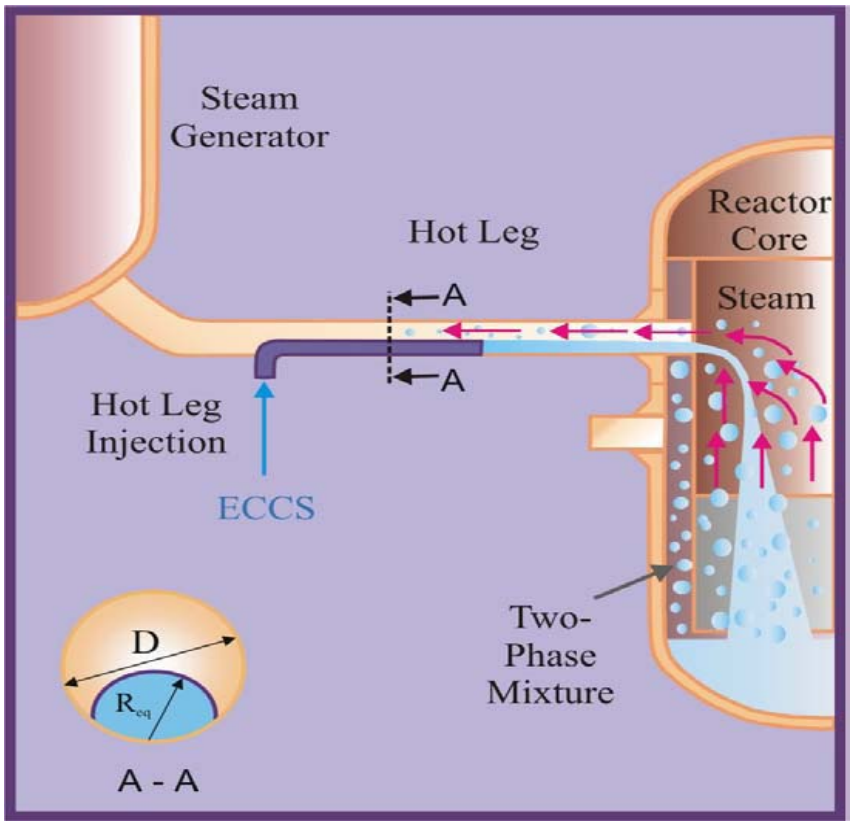

Fig. 1.6: Countercurrent flow of Steam & Cooling Water in Hot Leg of PWR during LOCA [5].

1.3 PRESSURE DROP: ROD BUNDLE & SPACERS

In the nuclear industry, pressure drop correlations find extensive applications for design & analysis of many systems and components. For example, validated pressure drop correlations are required to determine the extent of orificing needed to match the channel flow power, pumping power required, the riser height required to achieve a certain circulation rate in natural circulation BWRs, recirculation ratio in natural circulation type steam generators, stability analysis, transient & accident analyses, etc. Some of the above applications require correlations for both single-phase & two-phase flows. Two phase flows are encountered during normal operations of BWRs, transient & accidents in PWRs & PHWRs and in certain components like the steam generators. In a nuclear reactor, the generated power, $Q_{G,}$ is extracted from the core by means of a fluid coolant. The first purpose of the thermo hydraulic design of the reactor is to ensure that,

during the nominal steady state operating conditions, the extracted power, $Q_{E,}$ is equal to the generated one. Secondly, for accidental conditions, the evaluation of the difference between Q_G and Q_E is necessary for predicting the behaviour of the plant. The evaluation of the extracted power is performed by means of the well known relationship:

$$Q_E = W\Delta I \tag{1.1}$$

Where, ΔI is the enthalpy difference between the core outlet and inlet and W is the mass flow rate.

For the evaluation of the extracted power, it is then necessary to know the flow rate. In some cases, it can be measured (total flow rate in the main loop) but generally at the design level, it has to be computed & this calculation requires a knowledge of the pressure loss through the different parts of the plant.

Table 1.1 ***Factors affecting the pressure drop in rod bundles.***

Geometry	Basic shapes	Circular pipe, rectangular channel, annulus, etc.
	Other shapes & devices	Rod bundle, spacer, valve, heat exchanger, orifice , plenum, header pump etc.
Fluid status	Single phase	One- component Two component & multi component
	Two phase	
Flow nature	Laminar	
	Turbulent	
Flow pattern	Bubbly, slug, annular etc.	
Flow direction	Vertical up flow, down flow, inclined flow & horizontal flow	Co-current & counter-current flow
Operating conditions	Steady state Transient	
Driving force	Forced convection Natural convection	

1.3.1 COMPONENTS OF PRESSURE DROP

The total pressure loss, Δp comprises of three components, viz. ΔP_f, ΔP_l, ΔPe and ΔP_a which are components of pressure drop due to skin friction, form friction (also known as local friction), elevation and acceleration respectively. The skin friction pressure drop is also known simply as friction pressure drop. For the purpose of design of advanced reactors, the required correlations mainly cover the following configurations. For friction pressure loss, circular pipe, annulus and rod cluster and for local pressure loss, spacer, bottom and top tie plates, flow area changes like contraction, expansion, bends, tees, valves etc., are most common**[6]**.

a) Friction pressure drop: This is the irreversible component of pressure drop caused by shear stress at the wall and can be expressed as:

$$\Delta p_f = \frac{fL}{D_h}\frac{W^2}{2\rho A^2} \tag{1.2}$$

Where D_h is equal to 4 times flow area / wetted perimeter.

The pressure drop occurs all along the length and hence referred to as distributed pressure drop sometimes. This equation is applicable for single-phase and homogeneous two-phase flows, although, the method of calculation of the friction factor, f, and density,ρ, differ in the two cases. Pressure drop across tubes, rectangular channels, annuli, bare rod bundle (i.e. without spacers), etc., are examples of this component.

b) Local pressure drop: This is the localized irreversible pressure drop component caused by change in flow geometry and flow direction. Pressure drop across valves, elbows, tee, spacer, etc. are examples. The local pressure drop is given by

$$\Delta p_l = K\frac{W^2}{2\rho A^2} \tag{1.3}$$

Where, K is the local loss coefficient, the correlations for which differ for different geometries and for single-phase and two-phase flows.

c) Acceleration pressure drop: This reversible component of pressure drop is caused by a change in flow area or density. Expansion, contraction and fluid flowing

through a heated section are the examples. The acceleration pressure drop due to area change for single-phase and two-phase flow can be expressed as

$$\Delta p_a = \frac{(1 - A_r^2)\, W^2 \phi}{2 A_0^2 \rho_L} \tag{1.4}$$

Where A_0 = smaller flow area. $\phi = 1$ for single-phase flow and for two-phase flow ϕ is given by:

$$\phi = \left(\frac{x^3}{\rho_G^2 \alpha^2} + \frac{(1-x)^3}{\rho_L^2 (1-\alpha)^2} \right) \left(\frac{\rho_G \rho_L}{x \rho_L + (1-x) \rho_G} \right) \tag{1.5}$$

d) Elevation pressure drop: this reversible component of pressure is caused by difference in elevation & can be expressed as

$$\Delta P_e = \rho g \Delta z \cos\theta \tag{1.6}$$

Where, θ is the angle with the vertical in flow direction.

1.3.2 SPACERS

Spacer grids are a critical feature of all long fuel element assemblies and a weird and wonderful variety of types have been designed **[7]**. The functions and design requirements a spacer grid must fulfil are:

1) To maintain the required spacing of fuel pins within laid-down tolerances;
2) To prevent fretting corrosion or wear between fuel pin and spacer grid;
3) To permit free sliding of fuel pins to accommodate differential expansion;
4) To prevent the formation of steam voids or coolant flow distortion of a type likely to lead to local dry out, accelerated corrosion, cavitations or instability;
5) To minimize pin vibration;
6) To promote flow-mixing between sub-channels where required (e.g. PWR);
7) To resist forces involved during pin insertion and inertial loading during handling and transport;
8) To resist damage during charging into the core;
9) To have minimum neutron absorption.

This is a formidable list of requirements from which it is easy to understand why the spacer grid is at the heart of any successful assembly design. Since the spacers have a lot of shapes such as honeycomb-type, ring-type, and wire-wrapped-type and so on (Fig 1.7 & 1.8), it is difficult to predict the spacer loss without empirical correlations.

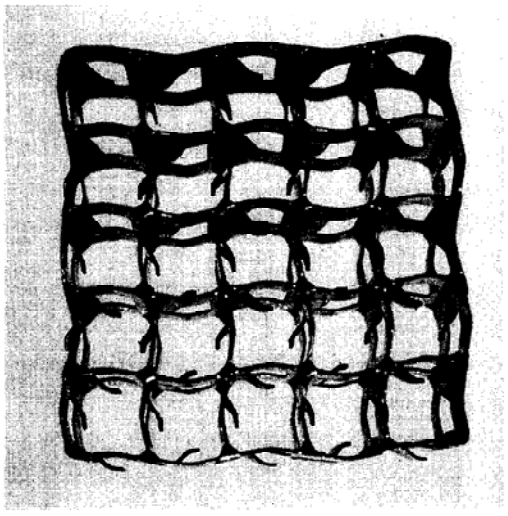

Standard spacer grid

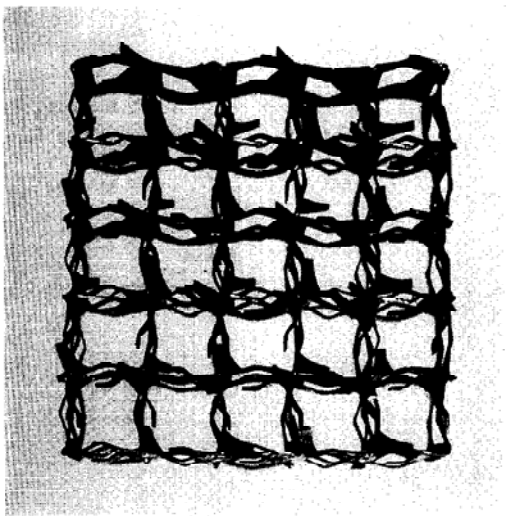

Wavy split vane spacer grid

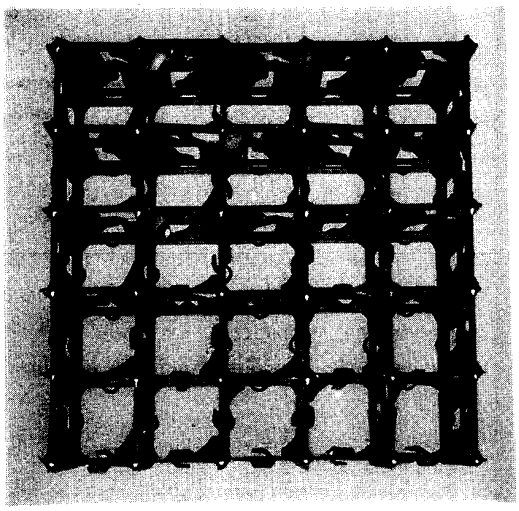

Inverted vane spacer grid

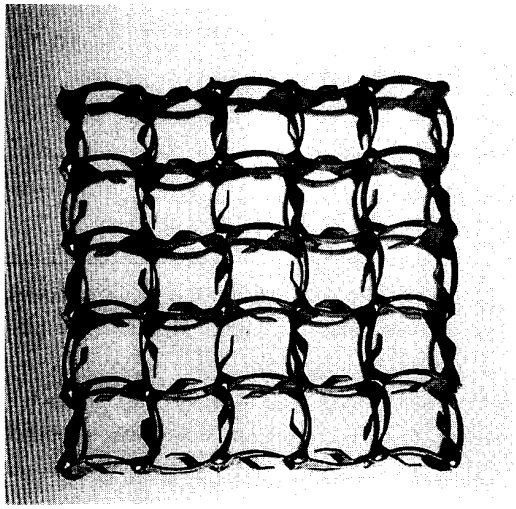

Inclined wave spacer grid

Fig. 1.7: Photographs of various spacer grids [8].

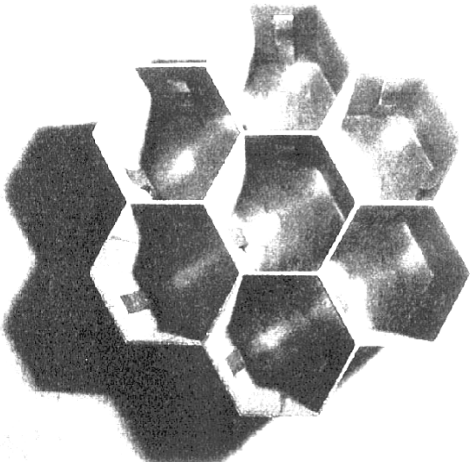

Honey comb spacer **[9]**

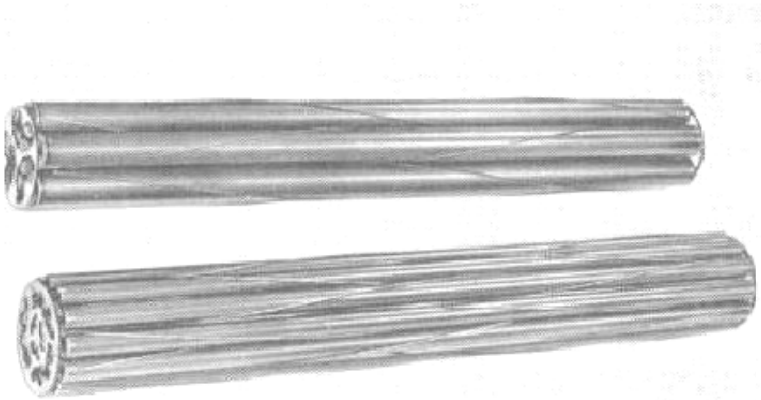

Wire wrap spacer

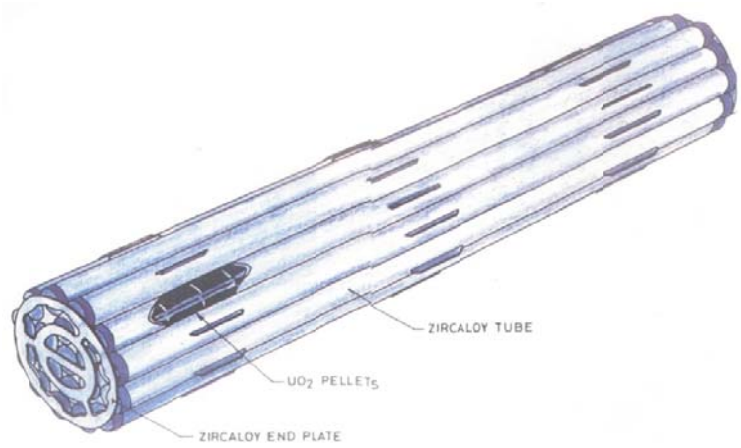

Split wart spacer

Fig. 1.8: commonly used spacer grids [7].

1.4 OBJECTIVE & ORGANIZATION OF THESIS

1. To study counter current flow phenomenon/flooding (air-water) and pressure drop in an annular geometry.

2. To derive a correlation for pressure loss coefficient at spacer and calculate the total pressure drop in D5 fuel cluster.
3. To design an experimental set up for study of flooding phenomenon.

The dissertation has been divided into six chapters with two appendices.

- Chapter 1 gives a brief introduction about the two phase flow, counter current flow phenomenon, components of pressure loss in a rod bundle, spacers and their geometries etc.

- Chapter 2 presents an extensive survey of the available literature regarding flooding phenomenon, pressure drop in rod bundles and various geometries of spacers as well as D5 fuel cluster.

- Chapter 3 enunciates a film thickness model for the falling annular film in annulus. A correlation to calculate the spacer loss coefficient and pressure drop in a fuel bundle based on flow area ratio has been discussed. Flow chart for the calculation of pressure drop in D5 fuel cluster with programming in MatLab is given.

- Chapter 4 discusses the design methodology of the proposed experimental set up for the study of flooding phenomenon. Design for liquid - air entry and exit ,liquid and air flow rate control devices have also been included in this chapter

- Chapter 5 describes the results of the film thickness model using a numerical programme in MatLab as well as the pressure drop in a D5 fuel cluster.

- Chapter 6 gives the nut shell of the studies made in above chapters as well as the scope for future work has also been outlined in this chapter.

****

CHAPTER 2

LITERATURE REVIEW

THEORETICAL MODELS AND CORRELATIONS

FLOODING MECHANISMS

GEOMETRICAL DEPENDENCIES

PRESSURE DROP: ROD BUNDLES & SPACERS

D5 FUEL CLUSTER

LITERATURE REVIEW

Numerous studies have been undertaken in phenomenon of the counter current flow limitation (CCFL) and pressure drop in fuel bundles and spacers. The literature can be classified into two categories: theoretical treatments and experimental investigation. In last few decades, several models have been proposed to predict the phenomenon of flooding. Each model seems to match the experimental data obtained by the researchers but seem to fail at different flow geometries and entry and exit conditions. Therefore, it is essential to unify the various models which can be used to predict flooding phenomenon. Additionally, a wide variety of correlations have been derived for the calculation of pressure drop in fuel bundles and spacers for different geometries like honey-comb, wire- wrapped, hexagonal etc.

2.1 THEORETICAL MODELS AND CORRELATIONS

Both theoretical & experimental investigations have been made to investigate the CCFL phenomenon and many models have been developed. The analytical models can be categorized in three groups as follows **[10]**:

- Wave dynamics model: Based on the idea that waves are developed on a liquid film and the waves become unstable to induce CCFL phenomena. [Richter, Shearer Davidson, Wallis & Kuo].
- Drop dynamics model: based on the idea that CCFL occurs when the gravity force exerted on a liquid drop is in a balance with the drag force by gas flow [Lee et al., McCarthy & Lee].
- Liquid film dynamics model: The velocity distribution of a liquid film is calculated, several models were developed at the condition that net liquid flow rate becomes zero and some models are at an instability condition of liquid film [Wallis, Bharathan et al.].

On the basis of theories it was concluded that the instability of counter current flow is manifested in several ways **[11]**:

- Sudden rise in the pressure gradient in the test section,
- Appearance of a sustained liquid flow above the liquid inlet,
- Reduction in the down flow rate of the liquid,
- Appearance of a highly disturbed film flow.

In general two flooding correlations have been vastly used in the research investigation of flooding phenomenon. The first is by Wallis based on the wave concept and relate dimensionless gas and liquid velocities at the flooding point **[12]**:

$$\left(V_L *\right)^{1/2} + \left(V_G *\right)^{1/2} = C \tag{2.1}$$

Where,

$$V_L* = \frac{\rho_L^{1/2} \upsilon_G}{\left[gD\left(\rho_L - \rho_G\right)\right]^{1/2}} \tag{2.2}$$

$V_L *$ = liquid dimensionless superficial velocity.

$$V_G* = \frac{\rho_G{}^{1/2} \upsilon_G}{\left[gD\left(\rho_L - \rho_G\right)\right]^{1/2}} \tag{2.3}$$

$V_G *$ = gas dimensionless superficial velocity, D is the diameter of the tube or in the case of annular sections it is the average circumference.

The second flooding correlation (Pushkina and Sorokin) is the Kutateladze number **[12]**. It specifies the point of zero liquid penetration at Ku_G = 3.2, where

$$Ku_G = \frac{\rho_G{}^{1/2} \upsilon_G}{\left[g\sigma\left(\rho_L - \rho_G\right)\right]^{1/4}} \tag{2.4}$$

$$Ku_L = \frac{\rho_L^{1/2} \upsilon_L}{\left[g\sigma\left(\rho_L - \rho_G\right)\right]^{1/4}} \tag{2.5}$$

The Kutateladze number has been derived from considerations of the stability of the liquid film and from the gas flow needed to suspend the largest stable drop. The Wallis correlation is found to predict flooding in pipe sizes up to 0.058 m in diameter and the Kutateladze number for pipe sizes larger than 0.152 m in diameter.

Flooding in annular sections has also been investigated because of its large use in nuclear down comers. The mechanism of flooding is similar to that of tubes however the characteristic length of diameter in tubes is replaced by the average annular circumference in annular geometries **[12]**. Equations of the Wallis **[13]** type for annular geometries are given by:

For 1/30 scale of a nuclear reactor down comer

$$V^{*1/2}_G + 0.8V^{*1/2}_L = 0.9 \quad (2.6)$$

For 1/15 scale of a nuclear reactor down comer

$$V^{*1/2}_G + 0.77V^{*1/2}_L = 0.8 \quad (2.7)$$

Suzuki & Ueda **[14]** experimentally studied the dependence of flooding gas velocity on various parameters – tube diameter, tube length, liquid flow rate, viscosity etc in circular tubes and disclosed that flooding phenomenon is caused by interaction between the waves on the liquid film and the upward gas stream.

Suzuki & Ueda [**15**] studied the phenomenon of flooding in annuli & rod bundles and introduced the concept of equivalent diameter of the channel. Using this diameter, the data for annuli & rod bundles are well correlated by the same empirical equation as that for circular tubes. He derived a flooding condition relating the maximum wave height to the gas velocity at the onset of flooding.

Richter [**16**] presented a new correlation for flooding which rule out the conflict between the Wallis correlation and the study done by Pushkina and Sorokin. This new correlation was found to be applicable for partial penetration of water both in pipe & annuli with the limitation that the liquid must travel down the pipe in the form of a film. The work done by Pushkina and Sorokin considered the effect of flooding on varying diameter pipe sections. They have characterized flooding as the point of no liquid penetration. They concluded that critical gas velocity for no liquid penetration was independent of pipe size. It is to be noted that their conclusion was valid for pipe sizes over 0.15 m in diameter. The second flooding correlation considered the effect of zero liquid penetration as well as the delivery of liquid as a function of gas flow rate. The experiments done by Wallis were valid for small diameter pipes. The results were that gas flow rate for zero penetration was proportional to the root of pipe diameter and increased with the pipe size. Equations are shown below:

$$j^{*1/2}_G + mj^{*1/2}_L = C \quad (2.8)$$

(Wallis Type flooding equation with j^*_G / j^*_L used instead of V_L^* and V_G^*, m and C are constants and m is approximately set to unity for two component systems when there is

no mass transfer between the phases. C is dependent upon entrance conditions and ranges usually between C=0.7 and C= 1.0 **[16]**. Pushkina and Sorokin suggested that the geometry of pipe does not depend on the onset of flooding. However, Wallis has shown a square relation for flooding velocity and pipe diameter. Richter [**16]** presented a correlation that is applicable over the entire test section range of Wallis and Pushkina and Sorokin with applicability to zero penetration as well as partial delivery in both tubes and annular geometries. The approach can be considered a semi-empirical method which is based on a force balance between the liquid and gas regions of a counter-current in annular flow regime. The onset of flooding was characterized by the destabilization of waves due to the pressure difference between wave crests and troughs not being balanced by surface tension. This result in droplets being broken off and transported co-current by the gas stream. The resulting equation resembled both the Wallis and Pushkina and Sorokin correlations when considered for different pipe diameters. By applying similar method to annular sections and replacing the diameter of the pipe with the average annular circumference following equations were obtained:

$$C_W N'^{3}_{B} J^{*6}_{G} S^{*2} J^{*2}_{L} + C_W N'_B J^{*4}_{G} + 150 C_W J^{*2}_{G} / S^{*} = 1 \qquad (2.9)$$

Where, C_W- wall friction factor, N'_B- Bond number, S- ratio of gap size to average circumference

$$N'_B = \left[\frac{D^2 g (\rho_l - \rho_g)}{\sigma} \right] \qquad (2.10)$$

Where, D is tube diameter.

Taitel and Barnea **[12],** developed a model for flow pattern prediction and transition for vertical counter-current gas-liquid flow as well as associated pressure drop. Taitel and Barnea used the Wallis **[13]** model for their no solution line on a flow map or instead the limit of counter-current flow. The equation is of the form:

$$\left[\frac{U_G \rho_G^{1/2}}{\sqrt{gD(\rho_L - \rho_G)}} \right]^{1/2} + \left[\frac{U_L \rho_L^{1/2}}{\sqrt{gD(\rho_L - \rho_G)}} \right]^{1/2} = C \qquad (2.11)$$

Where, U_{SG} and U_{SL} are superficial velocities of gas and liquid respectively and ρ_G and ρ_L are gas and liquid densities, g is the acceleration due to gravity, C is a constant

approximately equal to unity, and D is the pipe diameter. The liquid was in the form of a falling film for a range of gas flow rates up to the flooding point above which the down coming liquid is carried co-current to the gas steam. The gas velocity for no liquid penetration is obtained by setting the liquid term equal to zero and solving for the gas velocity. The flow pattern map for vertical counter-current flow is shown in Fig 2.1. The line 'a' is dependent on entry conditions and tube geometry. It may be mentioned that annular flow is the most natural flow pattern present in counter current flow. Taitel and Barnea **[12]** reported that no valid theory is available for the prediction of flooding process and relies on the empirical correlations.

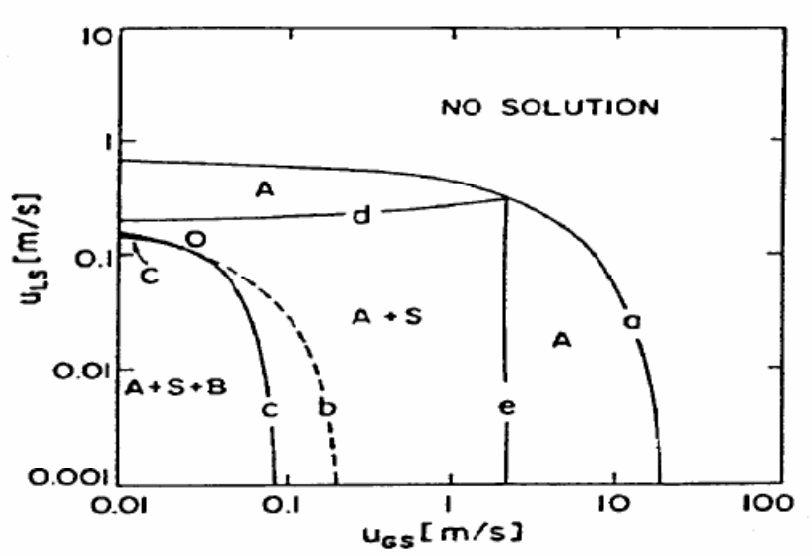

Fig. 2.1: Flow pattern map for vertical counter current pipe 5 cm in dia., air-water at 25^{0}C, 0.1MPa. A-annular, S-slug, B-bubble.

McQuillan and Whalley **[17]** performed a study to compare the flooding correlations and the test for gas-liquid flow in vertical pipes. Their study used a data bank of 2762 experimental flooding data points and 22 flooding correlations. The data bank contained the flooding information for various fluid properties and flow conditions and so offered a way of testing the span of precision and accuracy of the various correlations. The data bank was biased as far as fluid properties were concerned. The data bank includes water-air experimental data (68%) and small diameter tubes (78% less than 50 mm). The results of the comparison between the correlations and the experimental data were compiled and the measured differences presented were as follows:

- Empirical correlations performed better than theoretical correlations.
- Correlations that use dimensionless superficial velocities were less accurate compared to other empirical correlations especially when applied to high liquid rates and non air-water systems.
- The best theoretical correlation was one presented by Bharathan (1978). This equation was good over a range of liquid viscosities and surface tensions but over predicted flooding gas velocity for large diameter tubes.
- The best empirical equation was that of Askeev (1972). This equation performed well over a range of tube diameters and liquid surface tensions, but it over predicted flooding gas rates for high viscosities. The over prediction was corrected by McQuillan and an improved equation of the form:

$$Kg = 0.286Bo^{0.26} Fr^{-0.22} \left\{1 + \left(\mu/\mu_w\right)\right\} \tag{2.12}$$

Where,

Kg- gas Kutateladze number, Bo-Bond number, Fr-Froude number, μ-dynamic viscosity.

$$Fr = Q_l \left[\frac{g\left(\rho_l - \rho_g\right)^3}{\sigma^3} \right]^{1/4} \tag{2.13}$$

Lacey and Dukler **[12]** were concerned about the effects of entry region on flooding. They contended that the reason for the large disparities among flooding correlations was that previous research was not based on the physical mechanism that causes flooding. They conducted experiments in 50.0mm tubes and investigated the flow of liquid above and below the feed region. Their conclusion was that flooding occurred due the changes in the velocity profile of the film going from counter-current to co-current. That is, not by the previous mechanisms of upward wave propagation which result in liquid carryover or liquid bridging in the tube **[12]** resulting in gas forcing liquid ejection and hence flooding. This hypothesis is one that contradicts long standing accepted mechanisms of flooding. It is important to note that this is yet another example of experimental work done in single tube geometry for a specific fluid and so care must be taken when accepting this conclusion as a generic concept of flooding.

Y. Sudo **[19]** studied the mechanism of flooding & effects of predominant parameters regarding CCFL, adopting the criterion that the CCFL condition be given by an envelope of momentum equation applied for the entire length of the channel with respect to any void fraction. As a result he found that analytical model proposed could adequately predict all existing experimental results investigated in his study.

Vijayan et.al **[11]** experimentally studied the effect of tube diameter on flooding mechanism in vertical gas-liquid counter current annular flow. They found in lower diameter tubes it occurred by wave movement while in large diameter tubes (99 mm & 67 mm) it occurred by droplet carryover or by an unstable, churn- like motion in liquid film.

Mouza et al. **[20]** studied the falling film & flooding phenomenon in small diameter tubes by the liquids. He confirmed that the dominant mechanism is wave growth & upward dragging by the gas & that consequently the onset of flooding is strongly affected by liquid film structure.

Paras et al. **[21]** studied the liquid film characteristics & flooding phenomenon in counter current gas-liquid flow in a vertical narrow channel. He found that at low Re onset of flooding is associated with *liquid entrainment from isolated waves* while at high Re *local bridging* is dominant. He also presented a simple model for predicting the mean film thickness & mean wall shear stress counter – current gas-liquid flow below critical flooding velocities.

K. Saenmart et al. [**22]** experimentally investigated the onset of flooding for air & water in small diameter tube. They also discussed the effect of inclination on the onset of flooding.

Meyer and Giot **[23]** studied the counter current gas-liquid flows and in particular flooding phenomenon both theoretically and experimentally. Tests were performed in cylindrical (ID = 110 mm; length = 2 m) and annular geometries. The film thickness was measured by means of a conductance probe located inside the tube wall. The data obtained are well correlated by the classical expressions proposed by Wallis and Richter, as far as the flow rates are concerned. Therefore a new model based on a schematic

description of the wave pattern and motion has been developed. The main simplifying assumptions of the model are: (i) the waves are hemispherical and an average distance between successive waves can be defined; (ii) the liquid film thickness is determined by the end effects and by the gas flow rate; (iii) the liquid film between the waves is laminar; (iv) there is no slip between the waves and the surface of the underlying film; (v) the break-up of the waves corresponds to a critical Weber number.

2.2 FLOODING MECHANISMS

The mechanisms proposed to explain flooding and CCFL are discussed here. It has been suggested that all of these theoretical mechanisms can be reduced to three broad categories **[24]**. All other theories are considered to be variations on these three themes. As such, these mechanisms provide a comprehensive view of the factors which may or may not contribute to CCFL. The three major categories are:

1. Kinematic Waves
2. Upward Liquid Film Flow
3. Droplet Entrainment

2.2.1 KINEMATIC WAVES

The kinematic wave mechanism comes directly from the drift flux model of two phase flow. Wallis was the first to assign a drift flux solution to the flooding problem by examining the relative velocity of the phases to the drift flux. This model stipulates that the shear forces at the interface are negligible when compared to the gravity forces acting on the liquid phase. Kinematic waves are formed only by density differences and thus depend only on the continuity equation by definition, and as such do not depend on the momentum equation. As a result, acceleration and frictional pressure losses are also neglected from the analysis. Oshawa and Lahey have derived two terms that can be used to predict flooding.

$$\overline{jg} = \left(Co\,\bar{j} + \overline{Ugj}\right)\bar{\alpha} \tag{2.14}$$

Where $\bar{\alpha}$ is the average gas volume fraction. If the drift velocity, $\overline{U_{gj}}$, is only a function of physical properties and the average void fraction, we arrive at the following relationship for the drift flux:

$$\overline{j_{gf}} = \bar{\alpha}\left(\overline{u_g} - \bar{j}\right) \tag{2.15}$$

This final equation can be plotted and a graphical solution for $\overline{j_{gf}}$ can be found. Shown in Fig 2.2 **[24]**, the drift flux $\overline{j_{gf}}$ is dependent only on the void fraction if the velocities of the two fluids are known. The lines numbered one through four correspond to different values for the volume flux as indicated on the axes. The meanings of the lines are given below.

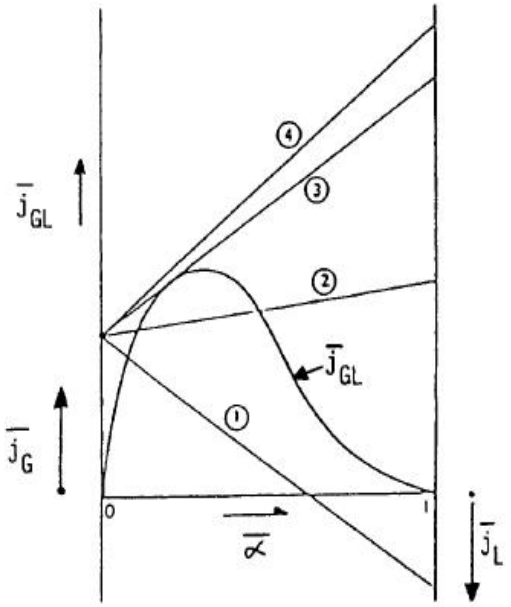

Fig. 2.2: Graphical Solution to Drift Flux problem [25].

- Line 1, Represents concurrent flow, from the figure it is obvious that the values for $\overline{j_f}$ and $\overline{j_g}$ are such that they maintain the same sign and thus are moving in the same direction.
- Line 2, Represents counter current flow without flooding. Again, the magnitude and direction of the terminus points of the line should indicate the directions of the fluid flows.
- Line 3, Represents CCFL. Line 3 is tangent to the curve and as such it is the only solution that results in a singular value for the drift ux.
- There is no intersection with the curve, physically impossible.

While this analysis does yield a very good approximation to the flooding problem, the curve shown above can only be constructed from experimentally gathered data. This is because there are three unknowns, j_f, j_g and α. As such, a fully deterministic prediction of flooding is not possible and this solution only provides a qualitative picture of CCFL.

2.2.2 UPWARD LIQUID FILM FLOW

The upward liquid film model makes use of dynamic waves as opposed to kinematic ones. Imura **[18]** states that a change in the wave amplitude on the surface of the fluid leads to bridging, which in turn leads to flooding. This theory is based on the belief that the process of flooding comes from the bridging of liquid across the cross section of the channel. This is also dependent, unlike the kinematic wave model, on the shear stresses acting on the interface between the gas and liquid phases. Cetinbudaklar **[26]** makes the case that the shear forces on the liquid interface can only be considered if the wave propagation is moving in the same direction as the gas flow due to the magnitude of the velocity.

Chung **[27]** admits that due to the rather complex nature of this analysis, the liquid film flow model lacks the acceptance of the Wallis and Kutateladze correlations. Taitel et al. make the case that if the interfacial shear terms are known or can be calculated, then characteristics of the flooding process can be found. They add that any entrance effects can be attributed to their effect on the interfacial shear, and thus on CCFL. This analysis was followed by an experimental investigation of Dukler concerning liquid film movement in vertical pipes. The claim is made that the upward shear on the liquid from the gaseous phase is sufficient to lift a liquid film upwards. The Reynolds number of the liquid film affects CCFL by contributing to a friction factor at the interface. Furthermore, this friction factor is related to the ratio of the film thickness and the tube diameter. Work by Barnea has suggested physical agreement with this theory.

2.2.3 DROP ENTRAINMENT

The droplet entrainment model was first mentioned by Dukler with respect to the momentum transfer of entrained droplets of liquid in the gaseous flow. It has been suggested that the small drops that are seen to be ripped from the surface of the fluid just before flooding occurs may lead to CCFL. The occurrence of flooding then becomes linked to a gas velocity that is capable of suspending the largest stable drop of water. This analysis is performed by conducting a force balance between the drag forces on a drop of water and the gravity forces acting on it as well. Moalem claims that this velocity can be found by means of the critical Weber number, We_c, and the drag coefficient of the drop, C_d.

$$U_g = \left(\frac{4\,We_c}{3C_d} \right)^{1/4} \left[\frac{\sigma g (\rho_f - \rho_g)}{(\rho_g)^2} \right]^{1/4} \tag{2.16}$$

Moalem further asserts that the results of such an analysis match the flooding correlation given by Sorokin et al. From these conclusions, the entrained droplet model does seem to offer a good approximation to the CCFL problem.

2.3 GEOMETRICAL DEPENDENCIES

The majority of geometric considerations concerning CCFL deal with the entrance configuration and flow mechanism of the liquid phase. Wallis was the first to recognize that entrance effects will change the conditions inside the test section. He discovered that flooding would occur more readily for a “smooth" entrance than for a “sharp" entrance. The smooth and sharp differentiation is with respect to the location where the liquid is entering the test section; that is, smooth indicates that the entrance ports were rounded flanges whereas sharp indicates a stepped flange entrance. Various liquid entrance & exit designs used for flooding study can be pictorially seen through figure 2.3(a-j) given below **[18]**.

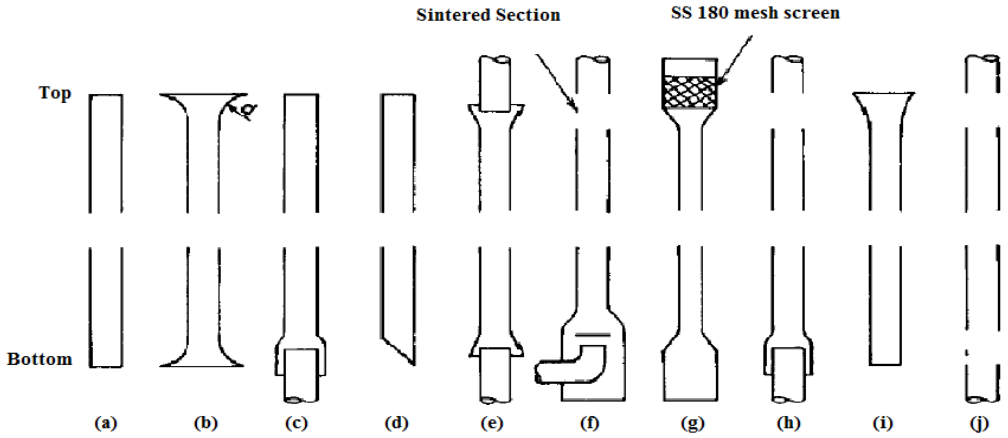

Fig. 2.3: Geometries of the tube ends (a) Wallis and Kusuda and Imura (b) Wallis (c) Kamer et al. (d) English et al. and Kusuda and Imura (e) Feind (f) Clift et al. (s) Grolmes et al. (h) Pushkina and Sorokin (I) Pushkina and Sorokin. (J) Hewitt and Wallis and Hewitt.

The geometry effect is further examined in detail by Chung **[27]** in which he concludes that the entrance and exit disturbances have an effect on the diameter dependence of the system. The result is that the constant values used in the Wallis correlation must be altered to allow for agreement. For the experiments he used, Chung suggests the Kutateladze constants, m and C_k can be adjusted according to the geometry.

However, Chung ultimately concludes that as the diameter of the test section increases the effect of entry conditions decreases. Finally, it has been suggested that much of the disagreement in the flooding data is a direct result of these separate entrance conditions.

The second important geometrical consideration is the actual test section diameter. The distinction between large and small diameter pipes with respect to CCFL was first made by Wallis. Wallis discovered that there does exist a dependence on diameter for the flooding point. This is most clearly illustrated by the definition of the Wallis dimensionless velocity which contains the pipe diameter as the characteristic length. This dependence on geometry is not specific to the transition from counter current flow to concurrent flow but between all flow regimes. The Pushkina study claims that there is no diameter dependence on the actual CCFL point other than the Bond number limit.

Numerous experimental investigation and analytical studies were conducted with respect to the accuracy of each correlation under separate diameters. It remains unclear as to what diameter should be used as a cut off point between the two correlations. Richter suggests the following cut offs: for pipes with an inner diameter up 50.8mm, the Wallis parameter should be used; for diameters greater than 152 mm, the Kutateladze should be used instead. Jayanti **[28]** claims the diameter dependence is limited to its effect on the two mechanisms for flooding; droplet entrainment and wave transport. The argument is that as the diameter of the pipe increases, the velocity of gas required to deliver liquid drops out of the test section is less than the gas velocity required to move a wave up the test section. There is no actual size given for this transition to take place.

Vijayan **[11]** attempted to reconcile this discrepancy by conducting similar experiments on several different pipe diameters. The final result of the study was that in tube diameters above 67 mm only the Kutateladze correlation should be used. Furthermore, Bankoff establishes that the diameter plays no part in the magnitude of the gas velocity if the dimensionless diameter, D^*, also described as the square root of the Bond number, is above 30.

$$D^* = D\left[\frac{g\left(\rho_f - \rho_g\right)}{\sigma}\right]^{1/2} \tag{2.17}$$

Based on this collection of knowledge on the topic of tube diameter and its relationship to flooding, it is concluded that the large diameter supposition is valid based on the findings of the above mentioned articles and the lack of any known contradictory data.

2.4 PRESSURE DROP: ROD BUNDLE & SPACERS

Rehme **[29]** did systematic investigations on the pressure drop for an incompressible, isothermal, fully developed turbulent flow in rod bundles with hexagonal arrangement of rods. The results of measurements of the pressure drop over a range of Reynolds numbers, Re = 6 x 10^2 - 2 x 10^5 in 25 test sections were communicated. The rods with rod distance ratios of P/D= 1.025-2.324 were surrounded by hexagonal channels. The number of rods was 7, 19, 27 and 61, respectively. On the basis of all results the following conclusions were summed up:

- A critical Reynolds number could not be detected for most of the test sections.
- The pressure drop coefficient quickly rises from approximately 60 percent of the circular tube value for closely packed rods ***(****P/D* = 1.0) to the circular tube value for *P/D = 1.08.* For even higher rod distance ratios, the pressure drop coefficients rise but a little to about 10% above the circular tube values at *P/D = 2.0.*
- The number of rods in a rod bundle has no measurable effect on the pressure drop coefficient.

Rehme **[30]** investigated the pressure loss at the several types of spacers experimentally. He indicated that the loss coefficient for the grid-type spacers is dependent on the relative plugging of a flow cross section, whereas the pressure loss coefficient for the wire-wrapped rod bundle is dependent on the lead of wire wraps.

Rehme & Trippe **[31]** did analysis of the pressure drop of turbulent flow through rod bundles. For laminar flow the dependence of the pressure drop on the pitch-to-diameter and wall-to-diameter ratios is discussed on the basis of theoretical analysis. In addition, they also presented correlations for the calculation of the pressure loss due to spacer grids and compared with experimental data. Rehme has defined the following parameters for the characterisation of rod bundles.

(a) Distance ratio of rods, *P/D*

(b) Distance ratio between the rods and channel wall, *W/D*

(c) Number of rods in the rod bundle.

Grover and Venkat Raj **[32]** investigated the pressure drop in three different designs of seven rod bundles having longitudinally finned rods. An analysis of the results indicated that in addition to the pitch-to-diameter ratio, wall distance to diameter ratio may also have an important influence on the friction factors. For clusters with finned rods an equivalent rod diameter can be an appropriate parameter for comparison of friction factor for rod clusters with that for smooth tubes on the basis of pitch-to-diameter ratio. The length of the spacer has been found to have a significant influence on the pressure drop across the spacer.

Saha et al. **[33]** at reactor division of BARC experimentally measured the pressure drop across various components of a pressurised heavy water reactor (PHWR) fuel channel under single-phase flow conditions. Empirical correlations were developed to predict the pressure drop for the various components of the fuel channel like rod bundles, end fittings, fuel locator and refuelling tools. They also studied the effects of bundle alignment at the junction and creep of fuel channels (both radial and axial) on pressure drop.

Masanori Aritomi et al. **[34]** investigated experimentally and analytically the effect of spacer geometry on the local pressure drop in a vertical circular channel using air and water as test fluids. Since the fuel spacer influences liquid film flow on fuel rods in BWR core, its specification has a strong effect on thermal hydraulics in the core such as critical power and pressure drop. Seeing this, the authors proposed a liquid film flow limitation model (narrow channel effect) in which the momentum balance of the liquid film phase in the near field of the spacer was considered. Modelling of local pressure drop of the spacer is required for closing the momentum equation. The authors considered that the following phenomena are dominant factors, which influence deposition rate distribution downstream of the spacer:

1. The ‘drift’ flow effect caused in the recovery process of flow splits due to the spacer.

2. A liquid film flow limitation due to the spacer (narrow channel effect).
3. The run-off effect induced by re-entrainment of a liquid film on the spacer surface, which is formed through droplet deposition.

G. Feldhaus et al. **[35]** studied the pressure drop, film flow rate and film thickness on a special test section modelling the four sub channels between ten fuel rods in LWR geometry with and without spacer grids. In the case without spacers, the results showed similar trends to data from tubular geometries with a similar hydraulic diameter. The two spacers tested both showed similar pressure losses. There was an increase in film flow rate and film thickness downstream of the ultra flow spacer. For a conventional egg-crate spacer there was a small change, with in some cases a decrease in film flow rate.

Kee-Nam Song et al. **[36]** devised their own spacer grid shapes. They compared their spacer grids with others on the spring characteristics, fuel rod vibration characteristics, fretting wear resistance, impact strength characteristics, CHF enhancement, and the pressure drop level of the spacer grid shapes from mechanical/structural and thermo hydraulic view points. The results show that the performances of newly developed spacer grid shapes are as good as or better than those of the commercial spacer grid shapes.

E. Bubelis & M. Schikorr [**37]** provided an overview of the existing wire-wrapped fuel bundle friction factor/pressure drop correlations and qualitatively evaluated which of the existing friction factor correlations are the best in retracing the results of a large set of the experimental data available on wire-wrapped fuel assemblies tested under different coolant conditions.

2.5 D5 FUEL CLUSTER

D5 fuel cluster is a cylindrical assembly of 4300 mm length and 118 mm diameter with fuel pins symmetrically distributed and it is used in AHWR (Advanced Heavy Water Reactor). AHWR is a thorium fuel based vertical pressure tube type reactor using D_2O as moderator and boiling H_2O as coolant in natural circulation mode. The arrangement of pins in the fuel cluster is shown in Fig 2.4. The cluster has 54 fuel pins arranged in 3 concentric rings around a central rod as shown in Fig. 2.5. The 24 fuel pins

in the outer ring have (Th–Pu) O_2 as fuel and the 30 fuel pins in the inner and intermediate rings have (Th–^{233}U) O_2 as fuel. The innermost 12 pins have a ^{233}U content of 3.0 wt. % and the middle 18 pins have 3.75 wt. % ^{233}U. The outer ring of (Th–Pu) O_2 pins contain 3.25 wt. % of total plutonium, of which the lower half of the active fuel has 4.0% Pu and the upper part has 2.5% Pu **[38].**

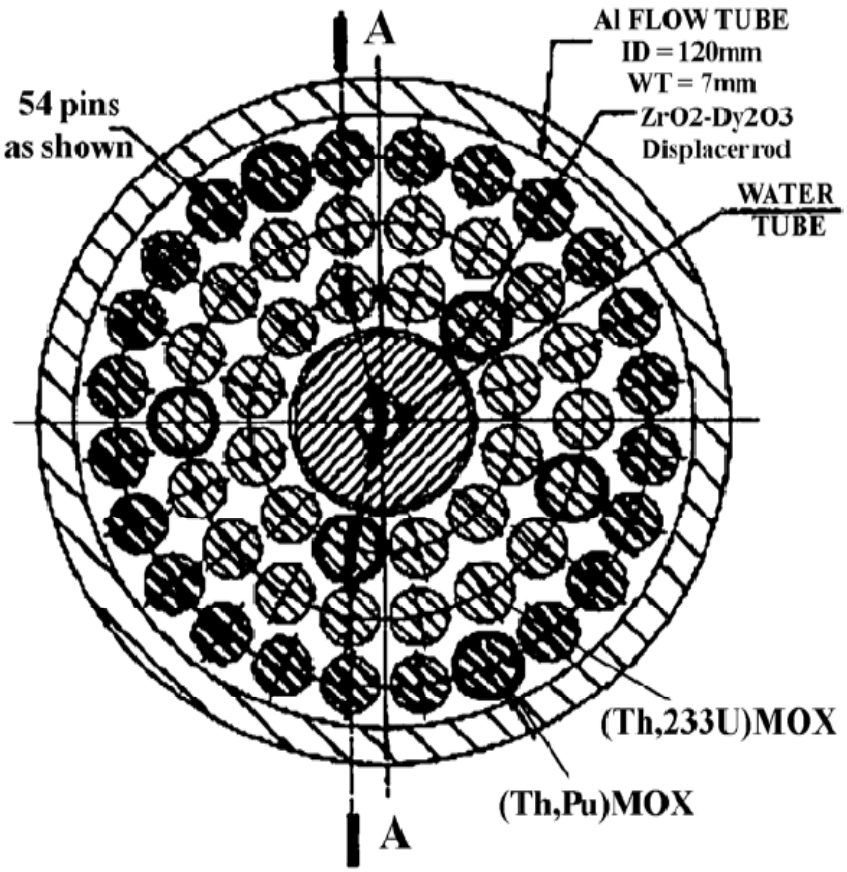

Fig. 2.4: Arrangement of 54 pin cluster [39].

The fuel pin consists of fuel pellets confined in a Zircaloy-2 clad tube. The fuel pin has a pellet stack length of 3500 mm and a plenum volume with a helical spring in it to keep the pellet stack pressed. The fuel pins are assembled in the form of a cluster with the help of the top and bottom tie-plates, with a central rod connecting the two tie-plates. Six spacers along the length of the cluster provide the intermediate pin spacing. The central rod has a tubular construction with holes for direct injection of ECCS water on the fuel rods **[38, 39]**.

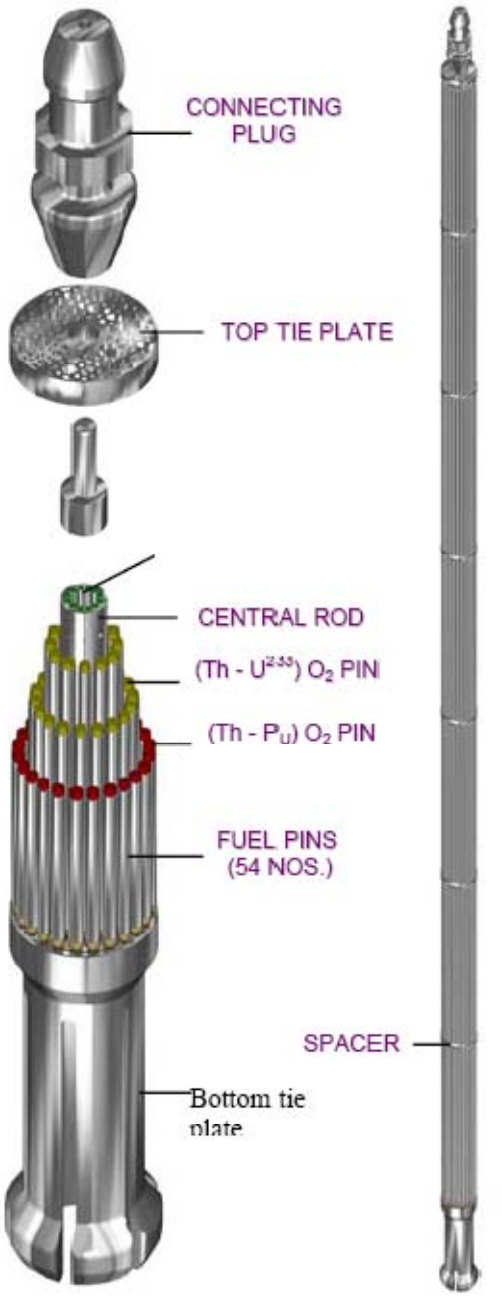

Fig. 2.5: AHWR D5 cluster details [39].

****

CHAPTER 3

ANALYTICAL STUDY

FLOODING CONDITION

FILM THICKNESS MODEL IN ANNULUS

PRESSURE LOSS COEFFICIENT AT SPACER

PRESSURE DROP CALCULATION IN D5 FUEL CLUSTER

ANALYTICAL STUDY

According to the study of the researchers and the literature cited in the course of this study, flooding takes place when a large amplitude wave is formed on the liquid film and carried upwards by the gas stream. At this condition, it is expected that part of the liquid is continuously torn off from the crest of the large amplitude wave and breaks up into droplets. As is well known, the liquid film is wavy and the pressure of the gas phase flowing on the wave crest is reduced due to the resultant acceleration of the gas flow. If the gas velocity is increased, the gas pressure on the crest decreases further because the wave amplitude becomes large with increasing gas velocity. In the range of low gas velocities, the wave on the liquid film is stable due to the surface tension acting on the wave surface. However, when the gas velocity is raised above a critical value, the pressure difference caused on the wave crest overcomes the surface tension. Therefore, flooding is thought to be connected with this force balance.

This chapter is divided into three parts. Part A comprises of mathematical condition for the flooding initiation as well as a mathematical model for the calculation of free falling film thickness in annulus. Part B consists of a simple mathematical correlation for the calculation of pressure loss coefficient at the spacer in fuel rod bundles based on flow area ratio. Parts C contain the steps to calculate the pressure drop in D5 fuel cluster and a programme is written in MatLab for the pressure drop calculation.

PART-A

3.1 FLOODING CONDITION

As a possible model, consider a state at the critical condition mentioned above. Figure 3.1 illustrates a liquid lump of a single large amplitude wave formed on the steady liquid film. Shape of the wave crest is assumed to be flat because the wave tip is continuously torn off by the gas stream. In this analysis the following assumptions are used;

1) Location of the liquid lump is fixed in space.
2) Shear stresses on the gas-liquid interface and the shroud surface are negligible excepting those on the liquid lump.
3) Both gravity force and compressibility of the gas phase are negligible.

In figure 3.1, Δh and δ_w, denote the height and width of the lump of large wave, p the pressure, A_G and A_L, U_G and U_L, ρ_G and ρ_L are the cross-sectional areas, mean velocities and densities of the gas and liquid phases, respectively.

Consider the variation of the gas phase pressure along the channel. The pressure loss Δp between the sections 1 and 2 can be expressed approximately as the sum of an abrupt contraction loss Δp_ζ and an abrupt expansion loss Δp_ξ at the section 0 **[23]**.

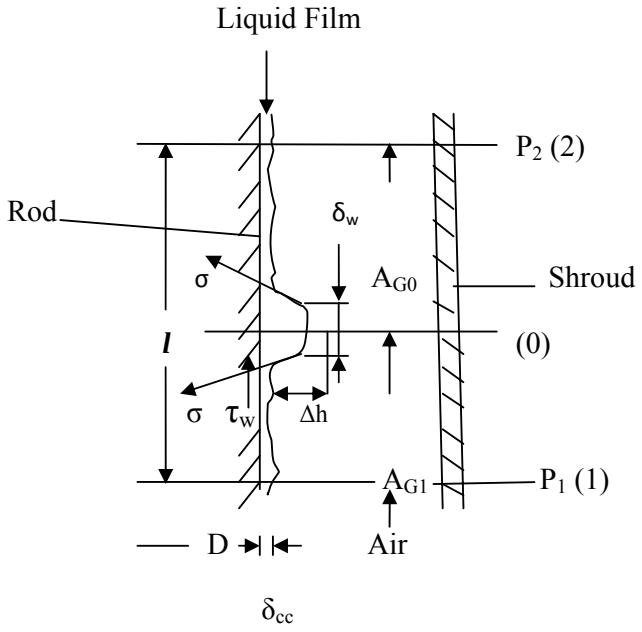

Fig. 3.1: Analytical Model.

The pressure loss **Δp** between the sections 1& 2 is given as

$$\Delta p = \Delta p_\zeta + \Delta p_\xi \tag{3.1}$$

Where, Δp_ζ = abrupt contraction loss at the section 0.

Δp_ξ = abrupt expansion loss at the section 0.

Abrupt contraction loss is given by

$$\Delta p_\zeta = \zeta_0 \frac{\rho_G}{2} U_{G0}^2 = \zeta_1 \frac{\rho_G}{2} U_{G1}^2 \tag{3.2}$$

Where, ζ_0, loss coefficient $= f\left(A_{G0} / A_{G1} \right)$

In the range of (A_{G1}/A_{G0}) = 0.4 - 0.85 **[15]**

$$\zeta_1 = (A_{G1}/A_{G0}) - 1$$

Therefore,

$$\Delta p_\zeta = \left[\left(\frac{A_{G1}}{A_{G0}}\right) - 1\right]\frac{\rho_G}{2}U_{G1}^{\ 2} \tag{3.3}$$

Abrupt expansion loss is given by

$$\Delta p_\xi = \xi\left(\frac{\rho_G}{2}\right)\left(U_{GO} - U_{G2}\right)^2 \tag{3.4}$$

As film thickness δ_{cc} is uniform except the liquid lump, then $A_{G1}=A_{G2}$ & $U_{G1}=U_{G2}$. By continuity equation at 1& 0, we get;

$$\frac{U_{G0}}{U_{G1}} = \frac{A_{G1}}{A_{G0}}$$

Therefore,

$$\Delta p_\xi = \left[\left(\frac{A_{G1}}{A_{G0}}\right) - 1\right]^2\frac{\rho_G}{2}U_{G1}^{\ 2} \tag{3.5}$$

Combining (3.1), (3.3) & (3.5); we get pressure drop across the channel

$$p_1 - p_2 = \Delta p = \frac{\rho_G}{2}U_{G1}^{\ 2}\left(\frac{A_{G1}}{A_{G0}}\right)\left[\left(\frac{A_{G1}}{A_{G0}}\right) - 1\right] \tag{3.6}$$

Applying Bernoulli's theorem between 1 & 0;

$$p_1 - p_0 = \frac{\rho_G}{2}U_{G1}^{\ 2}\left[\left(\frac{A_{G1}}{A_{G0}}\right)^2 - 1\right] \tag{3.7}$$

By force balance on liquid lump in horizontal direction,

$$(p_1 - p_0)\delta_w = \eta_c\sigma \tag{3.8}$$

Where, σ denotes the surface tension and

η_c factor depending upon the wave profile.

Therefore, when gas velocity is further increased i.e., $\mathbf{p0 \ll p_1}$, finally it results into **flood transition**.

In vertical direction applying the momentum equation to the sections 1& 2, the flow is steady, $u_{L1} = u_{L2}$ for the liquid film and $u_{G1} = u_{G2}$ for the gas stream, we get;

$$p_1(A_{G1} + A_{L1}) = p_2(A_{G2} + A_{L2}) + \pi D l \delta_{cc} \rho_L g + \pi(D + 2\delta_{cc})\delta_w \Delta h \rho_L g - \pi D l \tau_w$$

Where, D is the rod diameter and τ_w the shear stress on the rod surface. The shear stress on the inter face is so small that $\tau = \delta_{cc}\rho_L g$, therefore

$$\pi(D + 2\delta_{cc})\delta_w \Delta h \rho_L g = (A_{G1} + A_{G0})\Delta p \tag{3.9}$$

As, $\pi(D + 2\delta_{cc})\Delta h = A_{G1} - A_{G0}$ & $A_{G1} \gg A_{L1}$, the above equation can be written as follows:

$$(A_{G1} - A_{G0})\delta_w \rho_L g = A_{G1}\Delta p \tag{3.10}$$

From equation (3.6) & (3.9) wave width at onset of flooding is given as

$$\delta_w = \frac{\rho_G}{\rho_L}\frac{U_{G1}^2}{2g}\left(\frac{A_{G1}}{A_{G2}}\right)^2 \tag{3.11}$$

Finally substituting (3.7) & (3.10) into (3.8)

$$\eta_c = \left(\frac{\rho_G}{\rho_L}\frac{U_{G1}^2}{2g}\right)\left(\frac{\rho_G}{\sigma}\frac{U_{G1}^2}{2}\right)\left(\frac{A_{G1}}{A_{G0}}\right)^2\left[\left(\frac{A_{G1}}{A_{G2}}\right)^2 - 1\right]$$

Thus the profile factor is dependent on densities of fluid, surface tension, velocity of gas stream and area ratio.

3.2 FILM THICKNESS MODEL IN ANNULUS

In fig 3.2 liquid is falling on the outer periphery of the inner tube with flow velocity, $u_{L,}$ in a concentric tubular geometry in vertically downward direction and air is blowing from bottom to top in a counter current manner in the free annular space. Radial change in pressure is neglected. Let

δ_{cc} = film thickness in counter current flow situation

δ_{ff} = free falling film thickness in the absence of air

R = radius of the rod

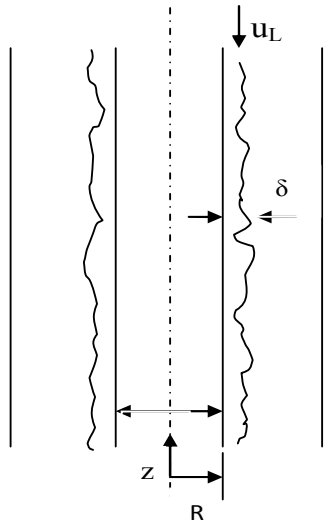

Fig. 3.2: Falling film in a circular annular geometry.

Assuming steady, laminar one-dimensional flow subjected to interfacial shear τ_i, the Navier strokes theorem in cylindrical coordinate reduces to the form

$$-\frac{1}{\rho_L}\left(\frac{\partial p}{\partial z}\right)+g+\frac{\mu_L}{\rho_L}\left[\frac{1}{r}\frac{\partial}{\partial r}\left(r.\frac{\partial u_z}{\partial r}\right)\right]=0 \qquad (3.12)$$

Boundary conditions:-

1) $u_z = 0$; r=R(no slip)

2) $\frac{\partial u_z}{\partial r} = -\frac{\tau_i}{\mu_L}$; r = R+δ_{cc}

The origin of coordinates is placed at the rod centre; r is radial distance from the rod centre & z is the axial coordinate of the rod along its length.

Integrating equation (3.12) with respect to "r"; we get

$$\frac{1}{2\rho_L}\left(\rho_L g - \frac{\partial p}{\partial z}\right) r^2 + \frac{\mu_L}{\rho_L}\left(r.\frac{\partial u_z}{\partial r}\right) = C_1 \qquad (3.13)$$

Applying the boundary condition (2) to above equation, we get:

$$C_1 = \left(\rho_L g - \frac{\partial p}{\partial z}\right)\frac{(R+\delta_{cc})^2}{2\rho_L} - \frac{\tau_i}{\rho_L}(R+\delta_{cc}) \qquad (3.14)$$

Putting the value of the constant C_1 in equation (3.13) gives the shear stress distribution as

$$\tau_{rz} = \left(\rho_L g - \frac{\partial p}{\partial z}\right)\frac{\{(R+\delta cc)^2 - r^2\}}{2r} - \frac{\tau_i}{r}(R+\delta_{cc}) \qquad (3.15)$$

The differential pressure drop of gas phase in r-z plane across a control volume of length "dz" can be written as

$$dp = \frac{\partial p}{\partial r}dr + \frac{\partial p}{\partial z}dz$$

As $\partial p/\partial r = 0$ & $\partial p/\partial z = \rho_G g dz = \text{constant}$, there the above expression reduces to

$$dp = \frac{\partial p}{\partial z}dz$$

Integrating between limits 1 & 2 in figure 3.1, we get

$$\frac{\partial \mathrm{p}}{\partial \mathrm{z}} = -\frac{(p_1 - p_2)}{l} \qquad (3.16)$$

Using equation (3.6) in above equation (3.16), we get

$$\frac{\partial p}{\partial z} = -\frac{\rho_G}{2l}\left(\frac{A_{G1}}{A_{G0}}\right)\left(\frac{A_{G1}}{A_{G0}} - 1\right)U_{G1}^2 \qquad (3.17)$$

Substituting equation (3.17) in equation (3.15) gives the following shear stress distribution

$$\tau_{rz} = \mu_L \frac{\partial u_z}{\partial r} = \left\{ \rho_L g + \frac{\rho_G}{2l}\left(\frac{A_{G1}}{A_{G0}}\right)\left(\frac{A_{G1}}{A_{G0}} - 1\right) U_{G1}{}^2 \right\} \left\{ \frac{(R+\delta_{cc})^2 - r^2}{2r} \right\} - \frac{\tau_i}{r}(R+\delta_{cc}) \tag{3.18}$$

Velocity distribution is obtained by integrating Eq. (3.18)

$$u_z(r) = [X]\left\{ (R+\delta_{cc})^2 \ln r - \frac{r^2}{2} \right\} - [Y]\{(R+\delta_{cc}) \ln r\} \tag{3.19}$$

Where,

$$[X] = \frac{1}{2\mu_L}\left\{ \rho_L g + \frac{\rho_G}{2l}\left(\frac{A_{G1}}{A_{G0}}\right)\left(\frac{A_{G1}}{A_{G0}} - 1\right) U_{G1}{}^2 \right\}, \quad [Y] = \frac{\tau_i}{\mu_L}$$

Liquid flow rate can be given by

$$Q = \int_R^{R+\delta cc} 2\pi r . u_z(r) dr$$

On simplification, flow rate is written as

$$Q = \frac{\pi}{4}\left[\begin{array}{l} \{X\}(R+\delta_{cc})^4 \{4\ln(R+\delta_{cc}) - 3\} - 2\{Y\}(R+\delta_{cc})^3 \{2\ln(R+\delta_{cc}) - 1\} \\ - \{X\}\left\{ 2(R+\delta_{cc})^2 (2\ln R - 1)R^2 - R^4 \right\} + 2\{Y\}(R+\delta_{cc})(2\ln R - 1)R^2 \end{array} \right] \tag{3.20}$$

Equation (3.20) can be reduced as;

$$Q = \frac{\pi}{4}[\{X\}(F) - \{Y\}(M) - \{X\}(E) + \{Y\}(N)] \tag{3.21}$$

Where,

$$F = (R+\delta_{CC})^4 \{4\ln(R+\delta_{CC}) - 3\}, \; M = 2(R+\delta_{CC})^3 \{2\ln(R+\delta_{CC}) - 1\}$$
$$E = \left\{ 2(R+\delta_{CC})^2 (2\ln R - 1)R^2 - R^4 \right\}, \; N = 2(R+\delta_{CC})R^2 (2\ln R - 1)$$

In the absence of air flow;

$$\{X\} = \frac{\rho_L g}{2\mu_L}, \{Y\} = 0, \delta_{cc} = \delta_{ff}$$

Finally flow rate, Q takes the form as below:

$$Q = \frac{\pi \rho_L g}{8\mu_L}[F - E] \tag{3.20}$$

Above equation can be further reduced as;

$$Q = C \times (F - E) \tag{3.21}$$

Where, $C = \frac{\pi \rho_L g}{8\mu_L}$

For the sake of numerical validation equation (3.21) can be written as

$$Q=B \tag{3.22}$$

Where, B=C*(F-E)

A numerical iterative procedure has been implemented for the validation of the derived film thickness model. Flow chart for the same has been given in figure (3.3).

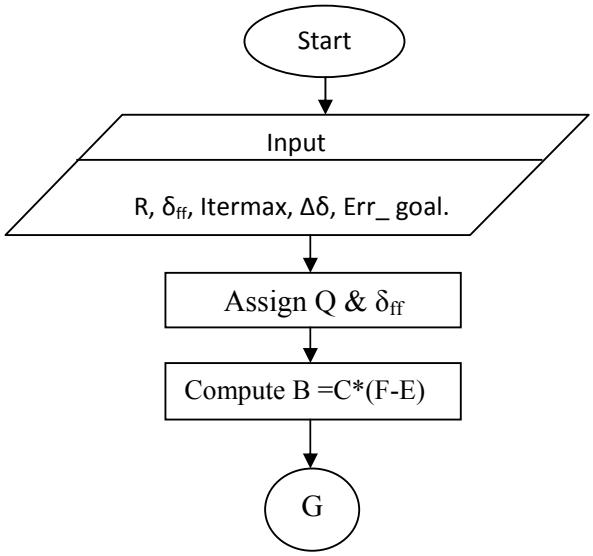

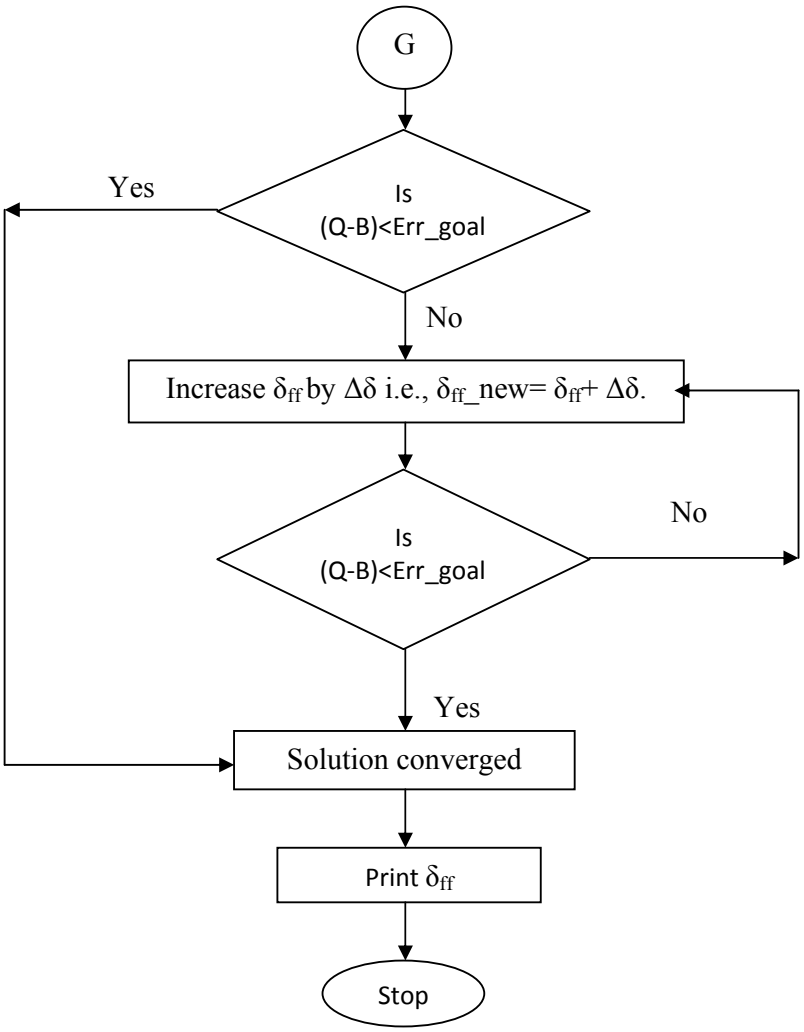

Fig. 3.3: Flow chart for the calculation of film thickness.

PART- B

3.3 PRESURE LOSS COEFFICIENT AT SPACER

An evaluation of the pressure loss at a spacer is important to enhance the prediction accuracy on pressure loss in multi-rod fuel bundles. Since, the spacers have a lot of shapes such as honeycomb-type, ring-type, and wire-wrapped-type and so on; it is difficult to predict the pressure loss at the spacer without empirical correlations. A simple evaluation method for the pressure loss at the spacer is therefore useful for the design of the reactor cores with multi-rod bundles. As shown in Fig.3.4, pressure loss at the spacer ΔP_{SP} can be expressed as a sum of the loss due to the contraction ΔP_C, the friction loss ΔP_F and the loss due to the expansion ΔP_E as follows:

$$\Delta P_{SP} = \Delta P_C + \Delta P_F + \Delta P_E \tag{3.23}$$

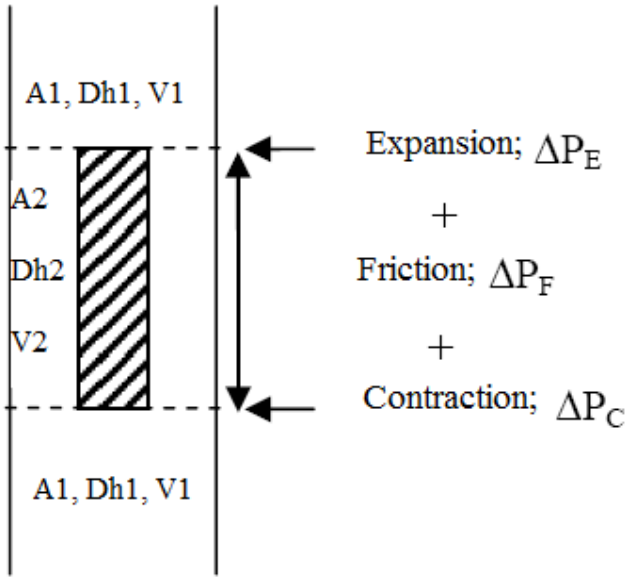

Fig.3.4: Schematic of pressure loss at spacer.

Each pressure loss is given by the mathematical correlation as

$$\Delta P_{SP} = K\frac{1}{2}\rho V_1{}^2 \tag{3.24}$$

$$\Delta P_C = \zeta c\frac{1}{2}\rho V_2{}^2 = \zeta c\left(\frac{A_2}{A_1}\right)^{-2}\frac{1}{2}\rho V_1{}^2 \tag{3.25}$$

$$\Delta P_F = f\frac{1}{2}\rho V_2{}^2\frac{L}{D_2} = f\left(\frac{A_2}{A_1}\right)^{-2}\frac{L}{D_2}\frac{1}{2}\rho V_1{}^2 \tag{3.26}$$

$$\Delta P_E = \zeta_E\frac{1}{2}\rho V_2{}^2 = \zeta_E\left(\frac{A_2}{A_1}\right)^{-2}\frac{1}{2}\rho V_1{}^2 \tag{3.27}$$

The subscript 1 denotes the normal flow section and 2 the flow section at the spacer, ρ, V, A represent the density of coolant, velocity of coolant, the flow area respectively, L the length of a spacer, D_h the hydraulic diameter, f the friction loss coefficient, ζ_C the coefficient of the pressure loss due to the contraction, ζ_E the coefficient of the pressure loss due to the expansion. Finally summing all the loss coefficients, we get the equivalent spacer loss coefficient as:

$$Keq = \left(\zeta c + f.\frac{L}{D_2} + \zeta_E \right)\left(\frac{A_2}{A_1} \right)^{-2} \tag{3.28}$$

Based on flow area ratio, IDELCHIK **[40]**, proposed the contraction & expansion loss coefficient in single phase flow to be as;

$$\zeta_C = 0.5\left(1 - \frac{A_2}{A_1} \right)^{0.75}$$

$$\zeta_E = \left(1 - \frac{A_2}{A_1} \right)^{2}$$

Equation (3.23) can be written as

$$Keq = \left[\left(0.5\left(1 - \frac{A_2}{A_1} \right)^{0.75} + f.\frac{L}{D_2} + \left(1 - \frac{A_2}{A_1} \right)^{2} \right) \right]\left(\frac{A_2}{A_1} \right)^{-2} \tag{3.29}$$

Above expression for pressure loss coefficient at spacer reveals its strong dependency on flow area and length.

'*f*', friction loss coefficient in Eq. (3.29) being a strong function of Reynolds number can be evaluated by the following correlation of tube flow.

$$f = \begin{cases} \dfrac{64}{\mathrm{Re}}; \mathrm{Re} \le 2300 \\ 0.316/\mathrm{Re}^{0.25} \text{ (Blassius)}; \mathrm{Re} > 2300 \end{cases}$$

Where; $\mathrm{Re} = \dfrac{\rho V De}{\mu}$; De= equivalent hydraulic diameter of rod bundle, given as

$$De = \frac{4A_1}{\pi\left(D_i + nD \right)}$$

Where, n = number of fuel rods, A_1 = normal flow cross section.

The total pressure drop of coolant in a fuel assembly or rod bundles can be empirically correlated as **[6]**

$$(\Delta P)_{FA} = (\Delta P)_f + (\Delta P)_{SP} + (\Delta P)_a + (\Delta P)_e \qquad (3.30)$$

Where, $(\Delta P)_{FA}$ = fuel assembly pressure drop

$(\Delta P)_f$ = frictional pressure drop, $(\Delta P)_{SP}$= spacer pressure drop

$(\Delta P)_a$ =acceleration pressure drop, $(\Delta P)_e$ = elevation pressure drop

Therefore, the final correlation for pressure drop in a fuel assembly given by Eq. (3.30) is expressed as

$$(\Delta P)_{FA} = \frac{1}{2}\left[f.\frac{L}{D_e} + N.Keq + \left(1 - Ar^2\right)\right]\rho V^2 + \rho g \Delta z \qquad (3.31)$$

Where, N = number of spacers, Ar (A_2/A_1) = flow area ratio (<1), ρ = density of coolant, V= coolant velocity, Δz = height of fuel assembly.

PART C

3.4 PRESSURE DROP CALCULATION IN D5 FUEL CLUSTER

Pressure drop in fuel cluster is broadly classified into two components - static and dynamic. Static component of pressure drop is due to the elevation and it contributes to major percentage of the total pressure drop in the fuel cluster. Pressure drop at spacers, frictional pressure drop along the fuel pin surface and pressure drop due to change of area, sudden expansion & contraction, valves, orifices, bundle junctions results in the dynamic component of pressure drop. It has always been the area of research how to minimize the pressure drop of the coolant. More is the pressure drop; higher will be the pumping power which results into reduced overall efficiency.

In D5 fuel cluster frictional pressure drop along the fuel pins is calculated using equivalent hydraulic diameter, De, concept. In general it is calculated mathematically by

$$D_e = \frac{4 * \text{flow area}}{\text{Wetted perimeter}}$$

The simulated D5 fuel cluster is shown in Fig. 3.5 below.

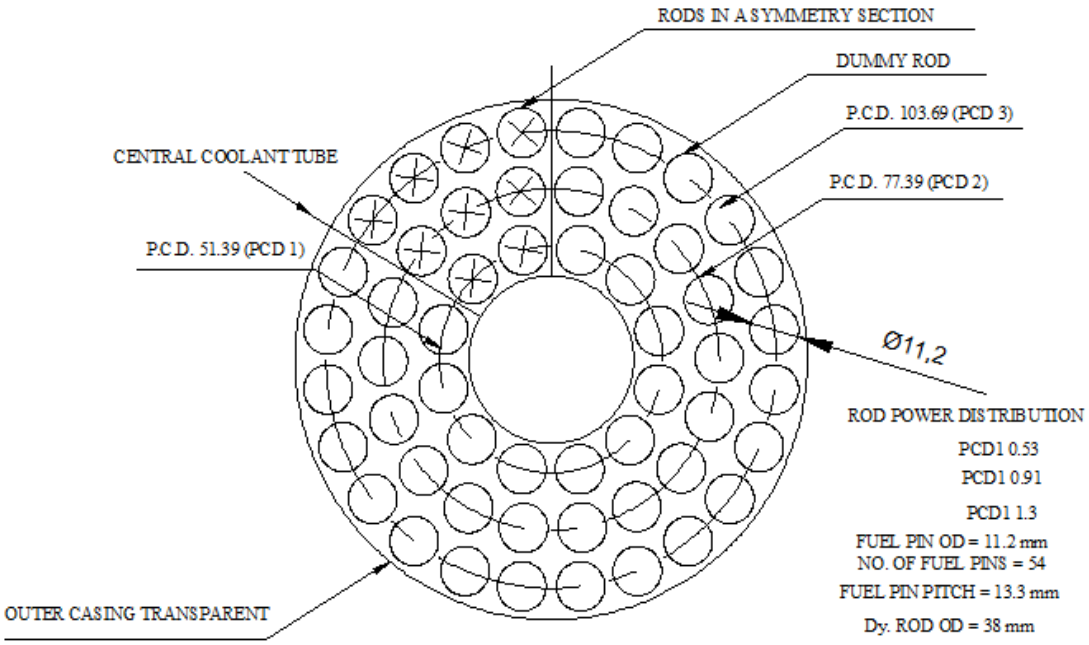

Fig. 3.5: Simulated D5 fuel cluster.

The arrangement of fuel pins at the spacer is symmetrical which is shown in Fig 3.6 below.

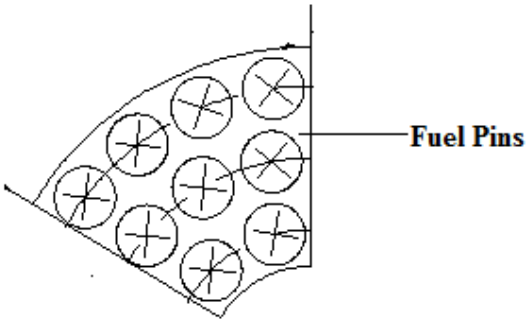

Fig. 3.6: Symmetrical distribution of fuel pins at spacer cross section.

The flow area for the calculation of spacer loss coefficient at and before the spacer in D5 fuel cluster in terms of diameters is mathematically correlated as;

$$A_1(before\ \ spacer) = \frac{\pi}{4}\left[\left(D_i{}^2 - D_{cr}{}^2\right) - 54D^2\right] \qquad (3.32)$$

Where, Di =shroud diameter, Dcr = coolant tube diameter, D= fuel pin diameter.

$$A_2(spacer) = \frac{\pi}{4}\left[\left(D_s{}^2 - D_{cr}{}^2\right) - 54D^2 - 54\left(D_{ho}{}^2 - D_{hi}{}^2\right) + \left(D_i{}^2 - D_s{}^2\right)\right] \quad (3.33)$$

Where, Ds = spacer diameter, D_{ho}= fuel pin hole outer diameter, D_{hi} = fuel pin hole inner diameter.

For D5 fuel cluster: A_1=8502.9 mm^2, A_2=5221.06 mm^2, Ar = (A_2/A_1) =0.614.

Equivalent hydraulic diameter, De = 14.6mm, hydraulic diameter at the spacer, D_2 =3.15mm. From experiments velocity of coolant is taken in the range of 0.0-0.20 m/sec.

Table 3.1 Spacer & fuel pin dimensions and coolant property.

S.No.	Parameters	Value
1.	Diameter of shroud, *Di*, mm.	139
2.	Diameter of spacer, *Ds*, mm.	118
3.	Diameter of coolant rod, *Dcr*, mm.	38
4.	Outer diameter of fuel pin rod hole, D_{ho}, mm	12.65
5.	Inner diameter of fuel pin rod hole, D_{hi} , mm	12.40
6.	Diameter of fuel pin rod, D, mm.	11.2
7.	Density of coolant (water), (Kg/m^3).	1000
8.	Viscosity of coolant (water), (N-sec/m^2).	0.001
9.	Number of fuel pins, n.	54
10.	Number of spacers, N.	6
11.	Height of the fuel assembly, m.	3.5
12.	Length of spacer, mm.	15

The flow chart for the calculation of pressure drop in a fuel assembly of D5 fuel cluster is shown in figure 3.7 below.

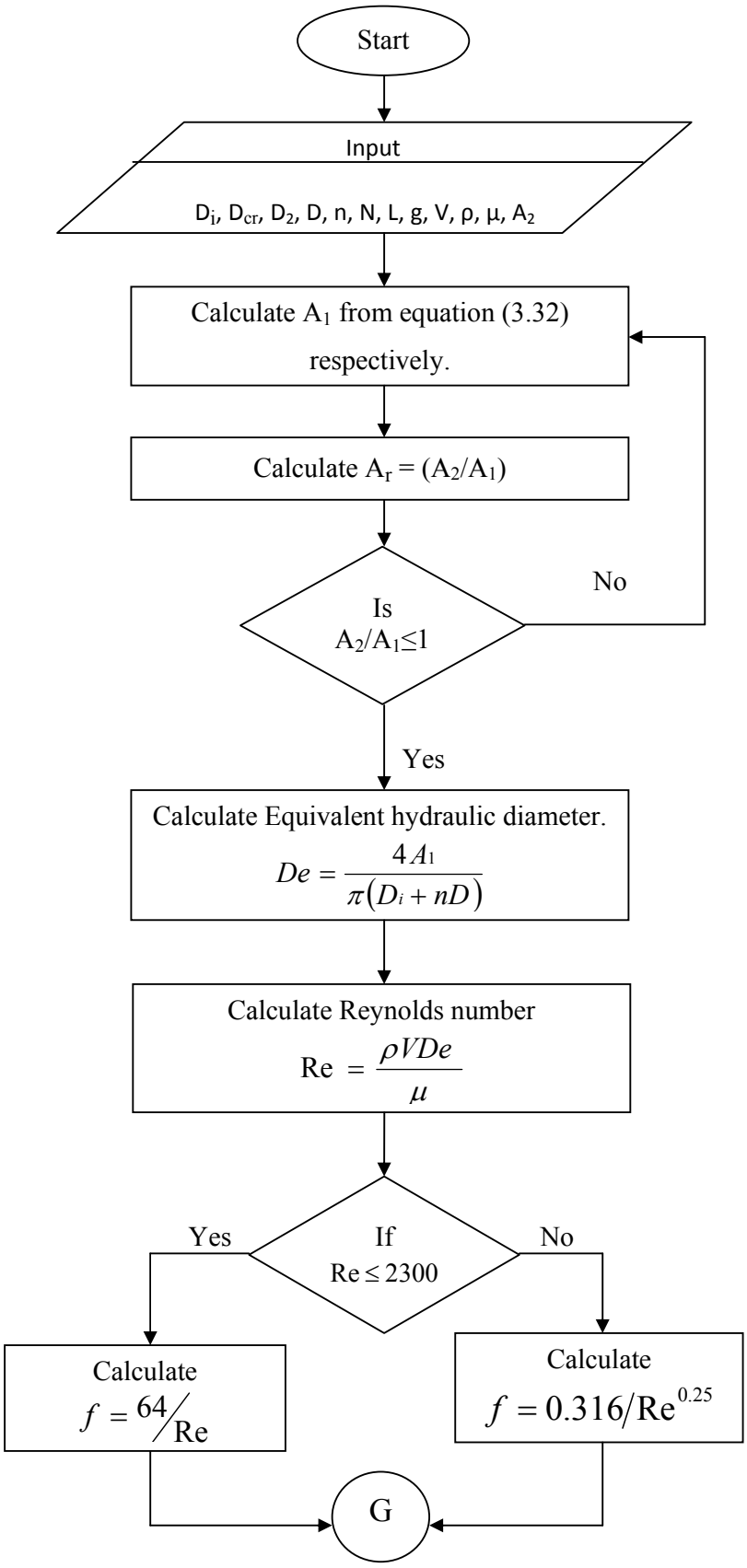
Start
Input
D_i, D_{cr}, D_2, D, n, N, L, g, V, ρ, μ, A_2
Calculate A_1 from equation (3.32) respectively.
Calculate $A_r = (A_2/A_1)$
Is $A_2/A_1 \leq 1$
No
Yes
Calculate Equivalent hydraulic diameter.
$De = \frac{4A_1}{\pi(D_i + nD)}$
Calculate Reynolds number
$\mathrm{Re} = \frac{\rho VDe}{\mu}$
If $\mathrm{Re} \leq 2300$
Yes
No
Calculate
$f = 64/\mathrm{Re}$
Calculate
$f = 0.316/\mathrm{Re}^{0.25}$
G

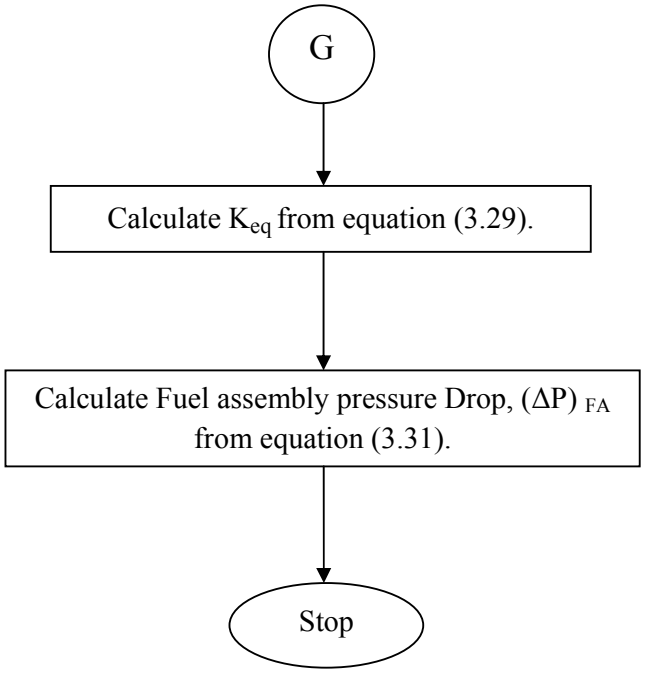

Fig. 3.7: Flow chart for the pressure drop calculation in D5 fuel cluster.

****

CHAPTER 4

EXPERIMENTAL DESIGN

SET UP DETAILS

INLET & OUTLET DESIGN

EXPERIMENTAL DESIGN

This chapter discusses on the design details of the proposed set up to be established for the experimental investigation of flooding mechanism and film thickness and its dependency on various geometrical and liquid parameters. This section details all structural and physical components of the experiment and provides both an explanation of the facility and an outline of the rationale for each component. This section is divided into several sections. First, the physical support structure, referred to as the "Structure" and its attachments is described. The next section is concerned primarily with the test section and all of its attachments and physical attributes. This section will deal with all parts of the experimental facility that are made from optically transparent Perspex. Finally, the third major section deals with the instrumentation and the data acquisition system. This section details all data gathering instruments and equipment including but not limited to electronic instruments (pressure cells, thermocouple, etc.) and manual equipment (rota meters). The schematic diagram of the experimental set up is shown in Fig 4.1.

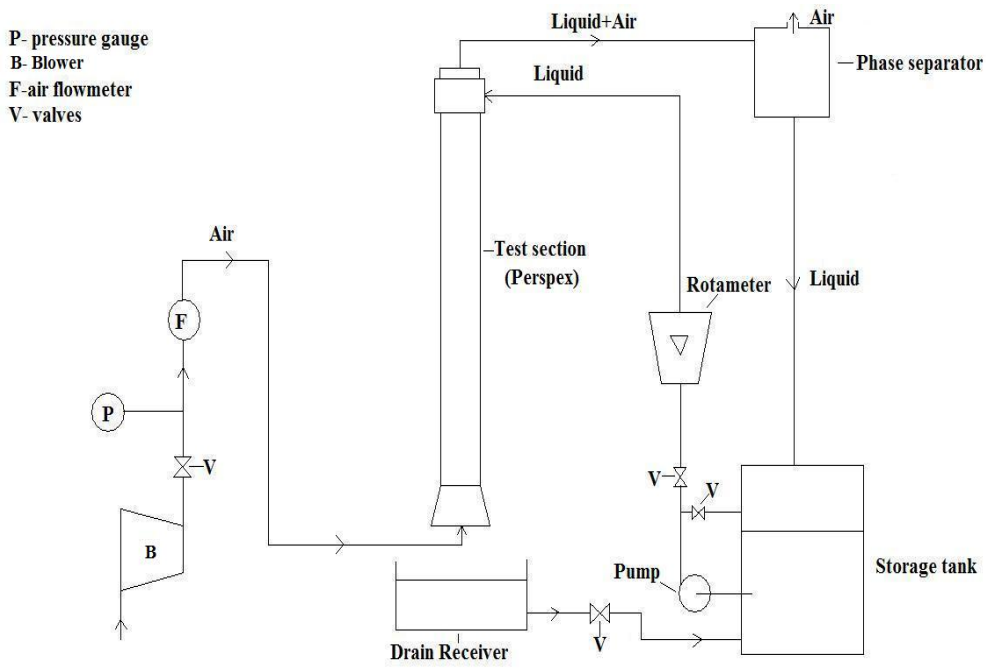

Fig. 4.1: Schematic of experimental set up.

Air and water is to be used as the working fluids. Properties of the fluids to be used in this study are enlisted in table 4.1. The main components of the system consisted of the test section, an air supply and a water supply. The test section, with an inside

diameter of 15 mm and the length of 1.5 m is to constructed from transparent acrylic glass to permit visual observation of the flow patterns. The connection of the piping system is designed so that the component part can be changed very easily. Water is pumped from the storage tank through a rota meter, to the water inlet section and hence flows back to the storage tank. The water inlet section (Fig 4.3) was constructed from two concentric tubes. The inner tube is radially drilled with 160 holes of 3 mm diameter. With this method, the water smoothly distributes along the tube. The water in the inlet section flowed downwards to the storage tank while the air flowed counter currently. The level of water in the water outlet section is constant, and the excess water returns to the storage tank. Air is supplied to the air inlet section and the test section by a blower. The air flow was controlled by a valve at the inlet of a flow meter. The inlet flow rate of air and water were measured by several sets of rota meter.

Table 4.1 ***Properties of fluids to be used in the set up***

S.No.	Fluids	σ (kg/sec2)	ρ (kg/m3)	μ (Pa-sec)
1.	Water	0.07118	1000	0.001
2.	Kerosene	0.0268	800	0.0014
3.	Air		1.2	0.000018

4.1 STRUCTURE

The "ground level" system upon which all other equipment is ultimately supported is the structural frame. This large structure provides both the physical grounding for the test section and instrumentation and also provides the rigidity needed for both stable operation and safety. This proposed structure is a five foot long by two foot wide by six foot high steel box made from 1-5/8 inch slotted steel channel. Standard fittings are used to connect all components and the structure is to be anchored to the concrete floor. The slotted channels allow for the attachment of other structural and non-structural components to the frame from two sides of the channel. The water delivery system is also located at the near end of the frame. This system includes the magnetic flow meter, the two manual control rota meters, and all associated piping and tubing. The location of the water delivery system minimizes the distance to the upper plenum of the test section for all inclination angles. All water is to be supplied by the building water main and feeds directly into the magnetic flow meter by way of a nominal one-half inch

pipe. From the flow meter, the water approaches the rota meters and is split in such a way that the flow meters receive an equal amount of water flow. Thus, the magnetic flow meter will provide all necessary flow data while the rota meters will allow for fine control. Water is circulated with the help of a centrifugal pump of capacity 1 horsepower.

4.2 ACRYLIC COMPONENTS

All parts of the experiment is to be constructed with optically transparent acrylic, better known as “Perspex” or those attaching to said acrylic are referred to as the test section. This distinction is necessary due to the fact that the actual “test section” is a 15mm inner diameter, 1.5 m long acrylic tube in which CCFL occurs. However, for ease of description, the convention in this section is to refer to all components directly attached or affected by this tube as the test section. It is necessary to briefly state all components which compose the test section and present a schematic view of the test section, shown in figure 4.2. Starting from the “top", i.e. those components located highest on the test section when it sits in a vertical position, there are: the air outlet assembly and flange, the upper plenum and flanges (which include all the water inlet ports and tubing), the test section tube (with associated flanges and pressure ports), the lower plenum and flanges, and the air inlet assembly (with associated fittings). The following subsections will detail the design of each listed component.

4.2.1 THE AIR OUTLET

The uppermost component of the test section is the air outlet. This component provides the air (and entrained water) a method of leaving the test section. The air outlet consists of two parts, the outlet body and a flange. The outlet body is a cast acrylic tube of 1/4-inch thickness. The end of the tube that lies inside of the test section has a 30 degree bevel on the inner surface. This bevel is added in order to reduce the flow resistance that the air would see as it leaves the test section. This design reduces the unwanted turbulent vortices and does not disturb the flow of incoming water through the holes radially drilled in the upper plenum of the test section.

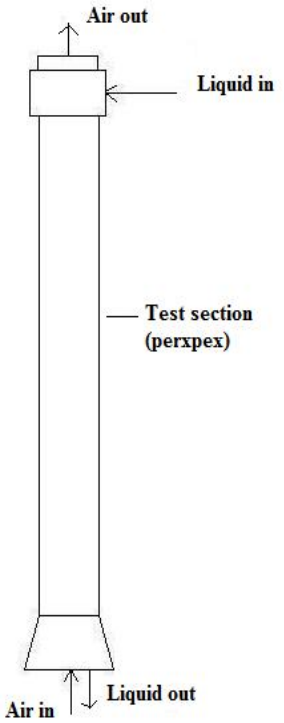

Fig. 4.2: Schematic of the test section showing the relative locations of the fluid inlets & outlets.

For the experiments to be conducted, the upper end of the air outlet is left open to the environment. This allows for the working fluids to exit the test section with a minimum of flow friction and acceleration pressure losses. The only friction seen by the fluids as they exit are wall friction and a slight reduction in flow diameter. This reduction in flow diameter, though, is small and does not contribute greatly to any inherent pressure drop. As a result, this component should not induce a significant pressurization of the test section. Thus, the pressure inside the test section can be assumed to be at atmospheric. The second purpose of the air outlet is to aid in the formation of annular flow. Since the air outlet tube rests inside of the test section, the end of which is situated below the holes which allow water into the test section, an annular film is formed within the test section.

4.2.2 UPPER PLENUM

The upper plenum of the test section provides the means by which the water enters the test section. It is an annular section with outside diameter 50mm, inside diameter 15mm and length 100 mm. Water first enters in this annular section through four injection points each of diameter 7.5 mm. It is collected in this hollow annular

chamber and then enters into the test section pipe through radially drilled regular hole of diameter 3mm on the outer periphery of test pipe inside the annular chamber. This helps in continuous wetting of test pipe on its inside surface from all directions in form of thin film of water. These four ports create an equal distribution of volumetric flow entering the upper plenum. The upper plenum provides the water pre-injection system for the test section. That is, water enters the plenum via the 7.5 holes, referred to as "injection ports", and comes to a relative fluid equilibrium, i.e. fixed gravity head and a fixed stagnation pressure. This results in the upper plenum acting as a stagnation chamber, allowing for the flow entering the test section holes to do so at relatively the same conditions. The exaggerated figure of water entry in upper plenum is shown in figure 4.3.

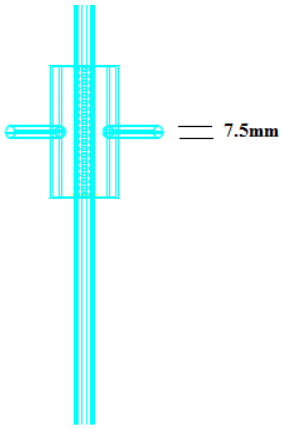

Fig. 4.3: Schematic of water entry in the upper plenum of test section.

4.2.3 TEST SECTION

The test section is the transparent acrylic tube in which CCFL is observed to occur. The test section used for this experiment measures 1.5m in length and has a nominal inner diameter of 15mm. The wall thickness of the test section is one quarter of an inch. Four pressure ports have been added, two on each side, to accommodate a differential pressure transducer and two absolute pressure transducers. On the upper end of the test section, inside of the upper plenum, the water enters the test section through a series of radially drilled hole of diameter 3mm. These holes are placed at the same axial plane and are radially symmetric. The water inlet of the test section directs the flow into an annular regime, alleviating many of the entrance effect problems. This water inlet configuration also allows for the symmetric entry of water into the test section. By

separating the flow into four distinct flow paths, the flow is evenly distributed around the test section. If, instead, the flow were allowed to enter the test section via slits cut into the tube, any flow disturbances induced by the water entering the upper plenum would be compounded and annular flow would not be maintained. The test section extends past the air inlet into the lower plenum. This configuration ensures that all of the air entering the test section will, at least initially, progress upwards into the test section after leaving the air inlet pipe.

4.2.4 LOWER PLENUM

The lower plenum is dimensionally identical to the upper plenum, but it does not have water injection ports. The primary purpose of the lower plenum is as a transfer tank for the water leaving the bottom of the test section. As such, it has no penetrations. This provides a good viewing chamber for both the water leaving the test section and the exhaust portion of the air inlet. Many important observations can be made by viewing these conditions while the test is running.

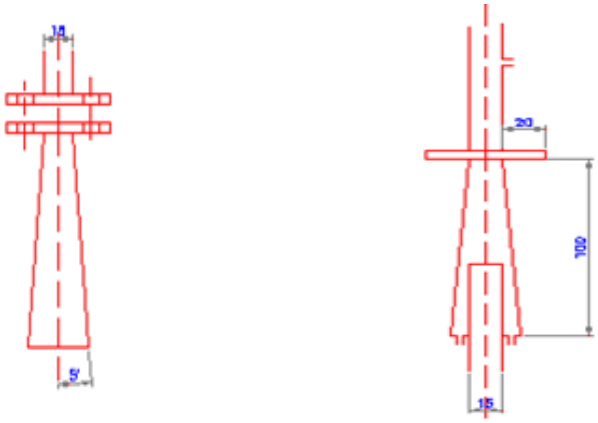

Fig. 4.4: Air inlet and liquid outlet

For liquid exit a divergent construction is provided which do two fold function. First it allows the water coming down before and after flooding to come down without any separation. Second it allows the air to flow in circular test section without any turbulence touching the water film. The length of the divergent part is 100mm and angle of divergence is 5 degrees.

4.3 INSTRUMENTATION

There are two major groups of instrumentation; the actual physical instrumentation and the data acquisition system. The setup of these two systems greatly affects the quality of the data taken and impacts the data taking process.

4.3.1 INSTRUMENTS & EQUIPMENTS

The instruments to be used in this experiment have been decided upon after taking inventory of the measurements that need to be recorded. Table 4.2 illustrates the quantities to measure and the type of measurement device to use. The liquid flow rate is the only measurement of the system that uses two devices in series. This is due to the fact that one of these instruments, the rota meters, serves a dual purpose as both a flow meter and as a control device. The error associated with the rota meters is additive across the two of them, and the error incurred by the two rota meters would be unacceptable. Therefore, in order to measure the liquid flow rate accurately a magnetic flow meter (Fig.4.5) is to be placed before the rota meters. The advantage of using magnetic flow meter is twofold. First its accuracy is much better than a simple rota meter and second, the magnetic flow meter also can be connected to the data acquisition system as it outputs a voltage signal proportional to the flow rate.

Table 4.2 ***Experimental measurements & Devices***

S.No.	Quantity	Measurement device
1.	Air velocity	Pitot tube
2.	Water velocity	Rota meters & Magnetic flow meters
3.	Pressure Gradient	Differential Pressure Transducer
4.	Upper Plenum Absolute Pressure	Absolute Pressure Transducer
5.	Lower Plenum Absolute Pressure	Absolute Pressure Transducer

Fig. 4.5: Magnetic Flow Meter

The air velocity measurement is to be made with the use of a pitot static tube system. The basic theory behind a pitot static tube air speed measurement states that if the stagnation pressure and the static pressure are known, from the Bernoulli equation, the dynamic pressure of the flow can be calculated.

$$\frac{\rho V^2}{2} + \rho g h + p = constant \tag{4.1}$$

Where, the fraction on the left hand side of the equation represents the dynamic pressure of the system. Also, the flow is assumed to be moving in streamlines so the change across them is zero, allowing for the 'ρgh' term to be assumed zero. This allows for equation 4.1 to be simplified into:

$$\frac{\rho V^2}{2} + P = P_0 \tag{4.2}$$

Where, P_0 is the "total pressure" of the system. With this in mind, a pitot static tube is inserted into an approach pipe leaving the blower at a distance sufficient for the flow to become fully developed. This probe contains both a pitot tube and a static pressure port which are then connected to a differential pressure transducer. The difference between their pressures is the dynamic pressure. The dynamic pressure is related to the velocity by the following relationship:

$$\Delta P_{dynamic} = \rho \frac{V^2}{2} \tag{4.3}$$

Thus a value is arrived at for the centreline velocity which can be related to the average velocity by a simple relationship. According to **[41]** the average velocity across the section of pipe is equal to two thirds of the maximum centreline velocity. Furthermore, the pressure transducer can also be directly connected to the data acquisition system and

the measurements automatically displayed and recorded. Both the upper and lower pressure ports on the test section will be measured using absolute pressure transducers. These are Honeywell model STA940 pressure transducers. The differential pressure measurement in the system is also made by way of a pressure transducer, a Honeywell STD924. The pressure transducer is a differential type and as such will measure the difference in pressure between the two pressure ports on the test section.

4.3.2 DATA ACQUISITION SYSTEM

The data acquisition system, or DAQ, to be utilized in this experiment consists of a Dell Precision Desktop connected to a National Instruments SCXI-1000 chassis. Within the SCXI-1000 chassis is a SCXI-1102b analog module connected to SCXI-1300 terminal block. Connected to the block are the data connections to the above described instruments. The physical specifications of the system as it is currently described allow for a data collection rate of well over 50 kHz. The high speed camera to be used for visualization is an X-Stream XS-4 CMOS camera with a resolution of 512*512. It has a maximum capture rate of 5000Hz.

****

CHAPTER 5

RESULTS & DISCUSSION

FILM THICKNESS MODEL VALIDATION

SPACER LOSS COEFFICIENT

PRESSURE DROP VERIFICATION

RESULTS & DISCUSSION

In this chapter, film thickness model developed to predict the thickness of free falling film in annulus has been validated with standard results using suitable numerical technique. The theoretical correlations developed to calculate the loss coefficient across the spacer and in fuel bundle have been compared with the experimental data and found satisfactory. The effect of flow area ratio on loss coefficient at spacer has been noticed as well as the effect of spacer geometry on spacer loss coefficient has been studied by varying the length of the spacer for different flow area ratios. Program has been written in MatLab to calculate the pressure drop in D5 fuel cluster using the developed correlations and the results have been compared with accepted results.

5.1 FILM THICKNESS MODEL VALIDATION

In this validation a numerical technique has been followed to obtain the film thickness for a particular flow rate using MatLab. A standard error or error goal, flow rate and maximum number of iterations have been defined. If for a particular flow rate the difference between the left hand & right hand side of equation (3.22) is less than the defined standard error or error goal, the iteration stops as the solution converges. If the difference does not become less than the defined standard error, film thickness is given a small increment keeping the flow rate constant and iteration starts till the solution converges i.e., difference between left and right hand side of equation become less than the standard defined error or error goal and the iteration continues up to the defined maximum number of iterations by incrementing the value of film thickness till the solution converges.

At lower flow rate film thickness increases but the curve tends to become constant at higher flow rates. This happens because at lower flow rates shear stress at wall is in balance with the weight of the falling film and falling film is in a state of free fall but at higher flow rate due to thickened film, drops are sheared off from the falling film under the action of gravity and film thickness tend to assume a constant value even if the flow rate go on increasing.

Table 5.1 below shows the variation of film thickness with increase in flow rate for falling films in the annulus as well as the number of iterations for the solution to converge for a particular flow rate.

Table 5.1 ***Comparison of theoretical & standard values of film thickness***

S.No.	Flow rate, Q (m^3/s)	No. of iterations	δth (m)	δ [A.Padhmanabhan]
1.	0.01	5	0.0006	0.0035
2.	0.02	11	0.0012	0.0044
3.	0.03	17	0.0018	0.0049
4.	0.04	23	0.0024	0.0056
5.	0.05	29	0.0030	0.0063
6.	0.06	34	0.0035	0.0068
7.	0.07	40	0.0041	0.0076
8.	0.08	45	0.0046	0.0082
9.	0.09	50	0.0050	0.0084
10.	0.1	58	0.0052	0.0086

From the table it is evident that the number of iterations increases with increase in the flow rate which shows the positive trend of the accepted scheme. At lower flow rates the increase in film thickness is faster but at higher flow rates this increase in film thickness is decreased and it tends to become constant. Column 5 in above table displays the results of film thickness in annular flow by Anand Padmanabhan **[1]**. Values are in congruence to that obtained by the theoretical film thickness model and show a positive trend of rise.

Figure 5.1 shows the plot between flow rate and film thickness for the free falling film thickness model.

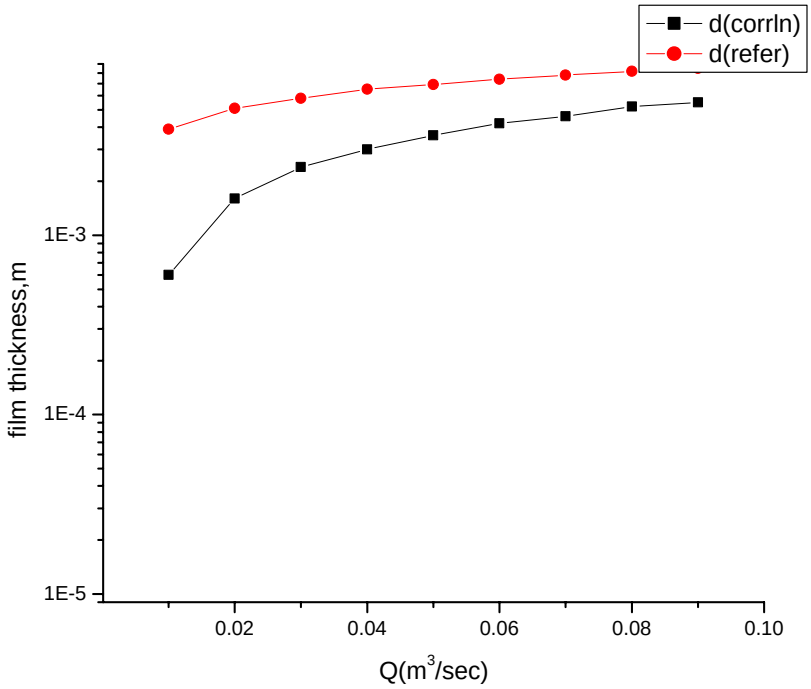

Fig. 5.1: Flow rate vs. Film thickness.

5.2 SPACER LOSS COEFFICIENT

Spacers in a fuel assembly results in an appreciable drop in pressure of coolant as well as the overall pressure drop in fuel assembly resulting due to elevation, acceleration of coolant, local change in areas etc., which results in a higher pumping power for the coolant. Though, this loss in pressure cannot be minimized to zero, but, it can be reduced to an appreciable amount by optimum design of spacer parameters such as length, diameter etc.

A general correlation to calculate the loss coefficient at spacer given by equation (3.29) based on flow area ratio has been derived and implemented to D5 fuel cluster and results have been compared with Rehme's data **[29,31]** who performed experiments with different geometries of spacers and fuel pin arrangements, where the trend of our plot is found to be satisfactory.

Table 5.2 contain the value of spacer loss coefficient calculated by the derived theoretical correlation (3.29) for two different lengths of spacers' viz., 15mm and 30 mm and compared with corresponding data of Rehme data bank for two different lengths.

Table 5.2 ***Spacer loss coefficient for varying spacer length and area ratio.***

S.No.	A2/A1	Equivalent Spacer Loss Coefficient (Keq)			
		L(15mm)		L(30 mm)	
		Kth	Kref	Kth	Kref
1.	0.5	3.001	2.855	3.83	3.456
2.	0.6	1.711	1.608	2.28	1.916
3.	0.7	1.01	0.958	1.43	1.193
4.	0.8	0.62	0.596	0.94	0.777
5.	0.9	0.372	0.398	0.63	0.542
6.	1.0	0.204	0.271	0.41	0.416

Variation of loss coefficient with respect to area ratio for different lengths has been shown graphically in the plot below(Figure 5.2).

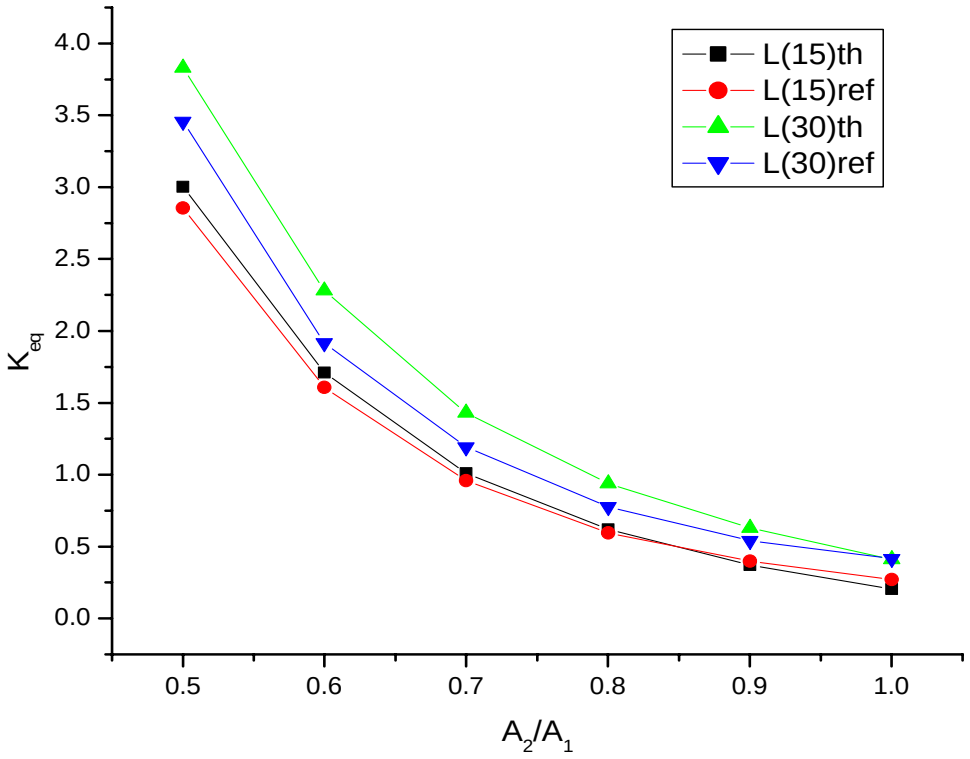

Fig. 5.2: Loss coefficient vs area ratio for different lengths of spacer.

From the plot it is visible that loss coefficient at the spacer decreases with increase in flow area ratio and is minimum when flow area ratio is unity i.e., a situation to be imagined without spacer. But at the same time it increases with the increment in the length of the spacer.

Taking into consideration the circularity of the rod bundle i.e., D5 fuel cluster, friction loss coefficient in rod bundle is calculated by using Blassius correlation. The variation of bundle friction factor with respect to reynolds number has been tabulated in the table 5.3 below. Reynolds number in this case has been calculated by using the equivalent hydraulic diamter concept **[15]**.

Table 5.3 ***Bundle friction factor at different Reynolds Number***

S.No	Reynolds No.	Bundle friction factor, f
1.	291	0.22
2.	582	0.109
3.	873	0.073
4.	1164	0.055
5.	1454	0.043
6.	1745	0.036
7.	2036	0.031
8.	2327	0.045
9.	2618	0.044
10.	2908	0.043

The plot between bundle friction factor with changing reynolds number based on equivalent hydraulic diamter concept is shown in figure 5.3.

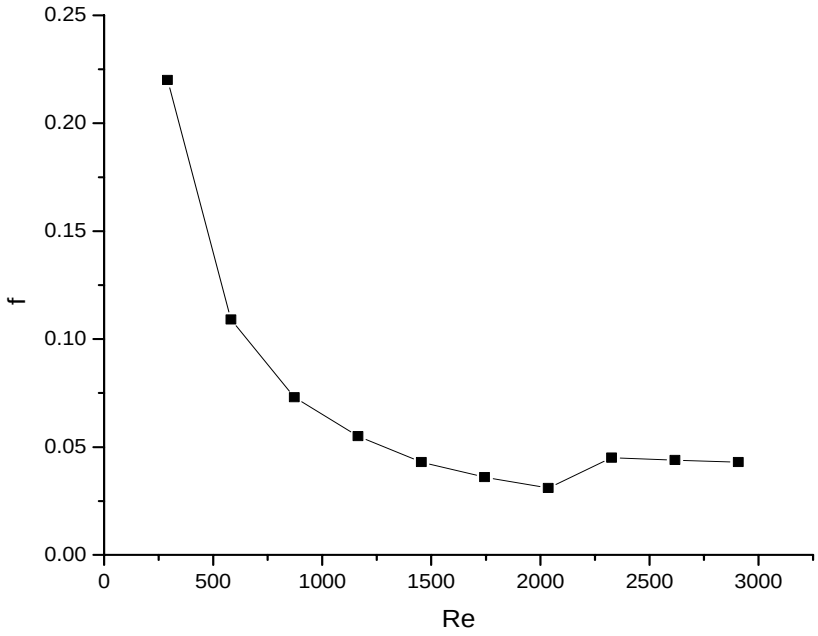

Fig 5.3: Bundle friction factor vs. Reynolds Number.

5.3 PRESSURE DROP VERIFICATION

The variation of pressure in D5 fuel cluster with coolant velocity is shown by figure 5.4.

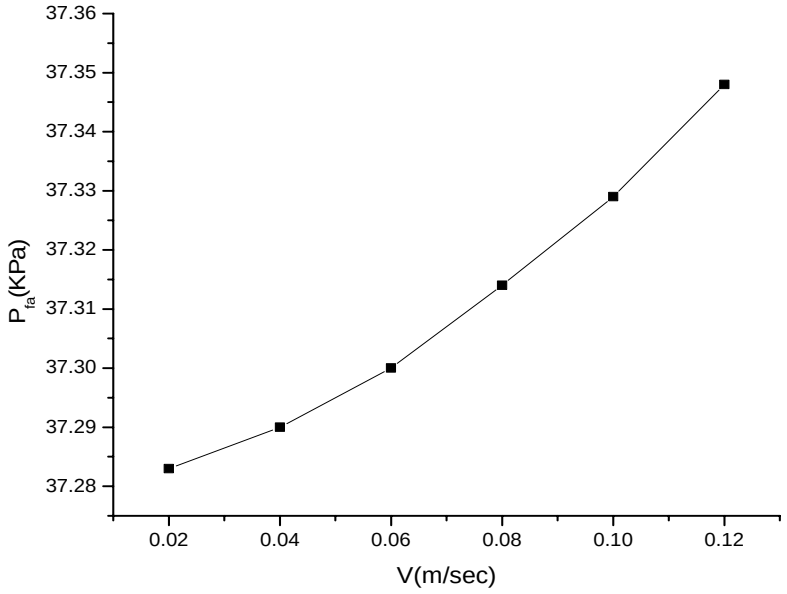

Fig. 5.4: Pressure drop in a D5 fuel cluster vs. coolant velocity.

The individual component of pressure drop due to acceleration, friction and spacer can be tabulated as under (Table 5.4).

Table 5.4 ***Component of individual pressure drop in D5 fuel cluster.***

S.No	V (m/s)	Friction Drop ΔP_f	Spacer Drop ΔP_{sp}	Acceleration Drop ΔP_a
1.	0.02	0.046	4.60	0.125
2.	0.04	0.090	11.60	0.498
3.	0.06	0.135	21.30	1.121
4.	0.08	0.180	33.40	1.994
5.	0.10	0.220	47.40	3.115
6.	0.12	0.260	65	4.486

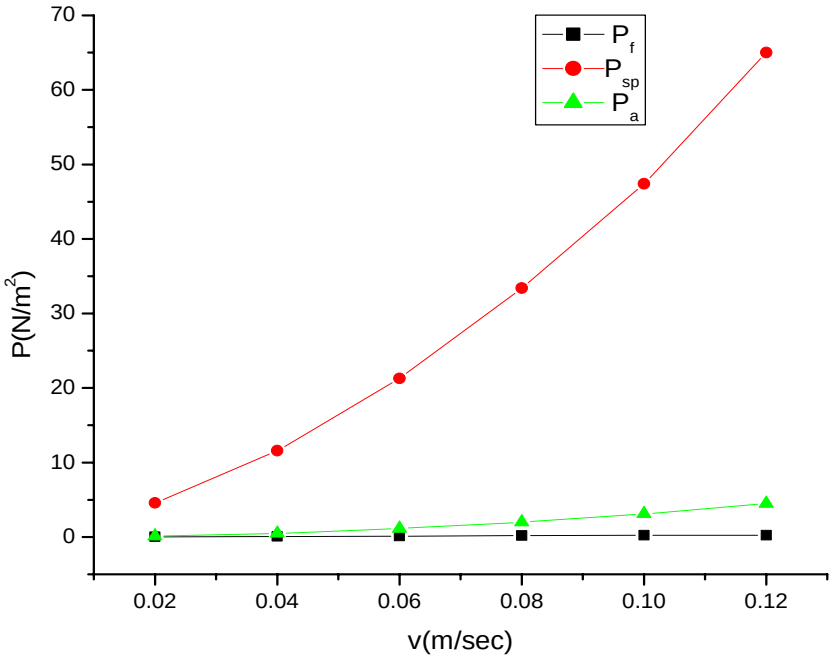

Fig. 5.5: Pressure drop components vs. coolant velocity.

CHAPTER 6

CONCLUSION &FUTURE WORK

CONCLUSION

An attempt has been made to investigate the gas liquid counter current flow phenomenon in an annulus of circular geometry. A film thickness model has been developed to estimate the film thickness in the annulus. Furthermore a theoretical model has been developed to evaluate the pressure drop at spacer plate in a D5 fuel cluster. The following conclusions are obtained from the present investigation and are as follows:

- The thesis presents a comprehensive review of literature on various aspects of gas liquid counter current flows, pressure drop in fuel bundle as well as spacers.

- A mathematical model has been developed to study the film thickness in a gas liquid counter current flow in a cylindrical annular geometry. A suitable numerical technique has been adopted to calculate the film thickness in the limiting condition of this model. The film thickness increases with increasing the coolant flow rate. The increase of film thickness is sharper at lower liquid flow rates compared to that of higher flow rate.

- A theoretical correlation based on flow area ratio has been developed to estimate the loss coefficients in fuel rod bundle. This has been implemented in a D5 fuel cluster to be used in AHWR (Advanced Heavy Water Reactor) to evaluate the overall static and dynamic pressure drop across various components of the fuel cluster. The results are compared to other available results and found to agree well with the available results.

- It is seen that significant amount of pressure drop takes place at spacers and found to increase with coolant velocity. A programme in MatLab has been written in order to evaluate the pressure drop in fuel cluster.

- The design of experimental set up for the study of gas liquid counter current flow along with instrumentation techniques to measure various parameters gas flow, liquid flow, film thickness has been proposed.

FUTURE WORK

Further investigation is required for the better understanding of the CCFL phenomenon. In view of this following studies are proposed for the future investigation:

- Concept of dimensional analysis may be implemented so that a dimensionless film thickness correlation may be developed.

- CFD modelling and experimental work is required to determine the hydrodynamic characteristics of falling films such as instantaneous velocity fields and wall shear stress. This is very challenging since the thickness of falling annular films are usually of the order of one millimetre.

- In the course of study of pressure drop in rod bundles, effect of entry and exit effects like pressure drop at base plate, tie plate may also be introduced as an appreciable loss takes place in these geometries.

****

REFERENCES

1) Anand Padmanaban. Film Thickness Measurements in falling annular Films, University of Saskatchewan, Canada, October **2006**.
2) Huawei Han. A study of entrainment in two-phase upward concurrent annular flow in a vertical tube, *Ph.D Thesis*. University of Saskatchewan, Canada, May **2005**.
3) W. A. Ragland and E. N. Ganic. Flooding in counter-current two-phase flow. Reactor Analysis and Safety Division, Argonne National Laboratory, Argonne, Illinois, U.S.A.
4) A. Zapke and D.G. Kroeger. Counter-current gas–liquid flow in inclined and vertical ducts—I: flow patterns, pressure drop characteristics and flooding. Int. J. Multiphase Flow **(2000)**, pp. 1439–1455.
5) M. Gargallo Gallego. Counter current flow limitations in horizontal stratified flows of air & water. *Ph.D thesis*. University of Stuttgart, Germany, **2004**.
6) Dilip Saha**.** Local phenomena associated with natural circulation. Bhabha Atomic Research Centre **(BARC)**, India.
7) D.O. Pickman. Design of Fuel Elements. Nuclear Engineering and Design 21 **(1972)** 303-317.
8) Jong Hee Cha and Hyung Gil Jun. Air- water flooding in multi rod channels: Effects of spacer grids and blockages. Journal of Korean Nuclear Society, Volume 25, Number 23, September **1993**.
9) Yasushi Yamamoto, Miyuki Akiba, Shinichi Morooka, Kenetsu Shirakawa and Nobuaki Abe. Thermal Hydraulic Performance of Tight Lattice Bundle. JSME International Journal, Series B, Vol. 49, No. 2, **2006**.
10) Ji Hwang Jeong. Development of counter current flow limitation model applicable to a sharp-edged liquid entrance. Korean journal of Chemical Eng., 18, 824-830 **(2001)**.
11) M. Vijayan, S. Jayanti, and A.R. Balakrishnan. Effect of tube diameter on flooding. Int. J. Multiphase Flow, 27**(2001)**:797-816.

12) Rishi R. Ramtahal. An experimental study of the applicability of flooding phenomena to the dynamic lubrication method of well control, *M.S Thesis*. Louisiana State University, December **2003**.

13) Wallis, G. B. **1969**, one dimensional Two- Phase Flow, McGraw-Hill, New York.

14) Suzuki and Ueda, **1977**. Behaviour of liquid films and flooding in counter-current two-phase flow—Part I. Flow in circular tubes. Int. J. Multiphase Flow, pp. 517–532.

15) T. Ueda and S. Suzuki. Behaviour of liquid films and flooding in Counter-current two phase flow. Part 2. Flow in annuli and rod bundles. Int. J. Multiphase Flow, Vol.4. pp. 157-170 **(1978)**.

16) Richter, H.J., **1981**. Flooding in tubes and annuli. Int. J. Multiphase Flow, pp. 647–658.

17) K.W. McQuillan and P.B. Whalley. Comparison between flooding correlations and experimental flooding data for gas-liquid flow in vertical circular tubes. Chem. Eng. Sci., 40**(1985)**:1425-40.

18) H. Imura, H. Kusuda, and S. Funatsu. Flooding velocity in a counter current annular two-phase flow. Chem. Eng. Sci., 32**(1977)**:79-87.

19) Y. Sudo. Mechanism and Effects of predominant parameters regarding limitation of falling water in vertical counter current two- phase flow. Journal of Heat Transfer, ASME, August **1996**, 716/ Vol.118.

20) A.A. Mouza, S.V. Paras and A.J. Karabelas, The influence of small tube diameter on falling film and flooding phenomena. Int. J. Multiphase Flow **(2002)**, pp. 1311–1331.

21) E. I. P. Droros, S.V Paras, A.J Karabelas. Counter-current gas-liquid flow in narrow channel- Liquid film characteristics & flooding phenomena. Int. J. Multiphase Flow (32) **2006** 51-81.

22) Krittapas Saenmart, Panachat Cheowuttikul, Adirek Suriyawong, Somchai Wongwises. Onset of flooding in small diameter tube. Int. J. Heat & Mass Transfer 35 **(2008)** 458-465.

23) B. Meyer and M. Giot. Experiments and modelling of flooding phenomenon. Nuclear Engineering and Design 99 **(1987)** 75-84.

24) Matthew A. Solomos. Experimental Investigation of the counter current flow phenomenon, Texas A& M University, **2008**.

25) Brennen, Christopher E. Fundamentals of Multiphase Flow. New York: Cambridge University Press, **2005**.

26) A.G. Cetinbudaklar and G.J. Jameson. The mechanism of flooding in vertical counter current two-phase flow. Chemical Engineering Science, 24**(1969)**:1669-1680.

27) S.K. Chung, L.P. Liu, and C.L. Tien. Flooding in two-phase counter current flows-II experimental investigation. Physicochemical. Hydrodynamics, 1(1980):209-220.

28) S. Jayanti, A. Tokarz, and G.F. Hewitt. Theoretical investigation of the diameter effect on flooding in counter current flow. Int. J. Multiphase Flow, 22**(1996)**:307-324.

29) K. Rehme. Pressure drop performance of rod bundles in hexagonal arrangements. Int.J. Heat .Mass Transfer. Vol. 15**(1971)**, pp. 2499-2517.

30) K. Rehme, Pressure drop correlations for fuel element spacers, Nuclear Technology 17 **(1973)** 15-23.

31) K. Rehme and G. Trippe, Pressure drop and velocity distribution in rod bundles with spacer grids. Nuclear Engineering Design 62 **(1980)** 349-359.

32) R.B. Grover and V. Venkat Raj. Pressure Drop along longitudinally-finned seven-rod cluster nuclear-fuel elements. Nuclear Engineering and Design 58 **(1980)** 79-83.

33) P.K. Vijayan, D.S. Pilkhwal, D. Saha, V. Venkat Raj. Experimental studies on the pressure drop across the various components of a PHWR fuel channel. Experimental Thermal and Fluid Science 20 **(1999)** 34 – 44.

34) Takashi Yano, Masanori Aritomi, Hiroshige Kikura, Hiroyuki Obata. Mechanistic modelling for ring-type BWR fuel spacer design 2. Local pressure drop and narrow channel effect. Nuclear Engineering and Design 205 **(2001)** 295–303.

35) G. Feldhaus, B.J. Azzopardi, W. Zeggel. Annular flow experiments in rod bundles with spacers. Nuclear Engineering and Design 213 **(2002)** 199–207.

36) Kee Nam Song, Soo-Bum Lee and Sang-Hoon Lee. Performance Analysis of new spacer grid shapes for PWRS. Korea Atomic Energy Research Institute (KAERI), 2007.

37) E. Bubelis, M. Schikorr. Review and proposal for best fit of wire-wrapped fuel bundle friction factor and pressure drop predictions using various existing correlations. Nuclear Engineering and Design 238 **(2008)** 3299–3320.

38) R.K. Sinha, A. Kakodkar. Design and development of the AHWR—the Indian thorium fuelled innovative nuclear reactor. Nuclear Engineering and Design 236 **(2006)** 683–700.

39) B. Bhattacharjee. An Overview of R&D in fuel cycle activities of AHWR. Bhabha Atomic Research Centre **(BARC)**, India.

40) Nilokev Ivanov Kolev. Multi phase Flow Dynamics 2: Thermal & Mechanical Interactions. New York: Springer Verlag, **2007**.

41) R.W. Fox and A.T. McDonald. Introduction to Fluid Mechanics. John Wiley & Sons New York, **1985**.

42) S. Jayanti, A. Tokarz, and G.F. Hewitt. Theoretical investigation of the diameter effect on flooding in counter current flow. Int. J. Multiphase Flow, 22**(1996)**:307-324.

43) Hidesada Tamai, Masatoshi Kureta, Akira Ohnuki, Takashi Sato and Hajime Akimoto. Pressure Drop Experiments using Tight-Lattice 37-Rod Bundles. Journal of Nuclear Science and Technology, Vol. 43, No. 6, p. 699–706 **(2006)**.

44) Hidesada Tamai, Masatoshi Kureta, Hiroyuki Yoshida and Hajime Akimoto. Pressure Drop Characteristics in Tight-Lattice Bundles for Reduced-Moderation Water Reactors. JSME International Journal, Series B, Vol. 47, No. 2, **2004**.

45) Zapke, A. and Kroeger, D.G., **1996**. The influence of fluid properties and inlet geometry on flooding in vertical and inclined tubes. Int. J. Multiphase Flow, pp. 461–472.

****

APPENDIX 1

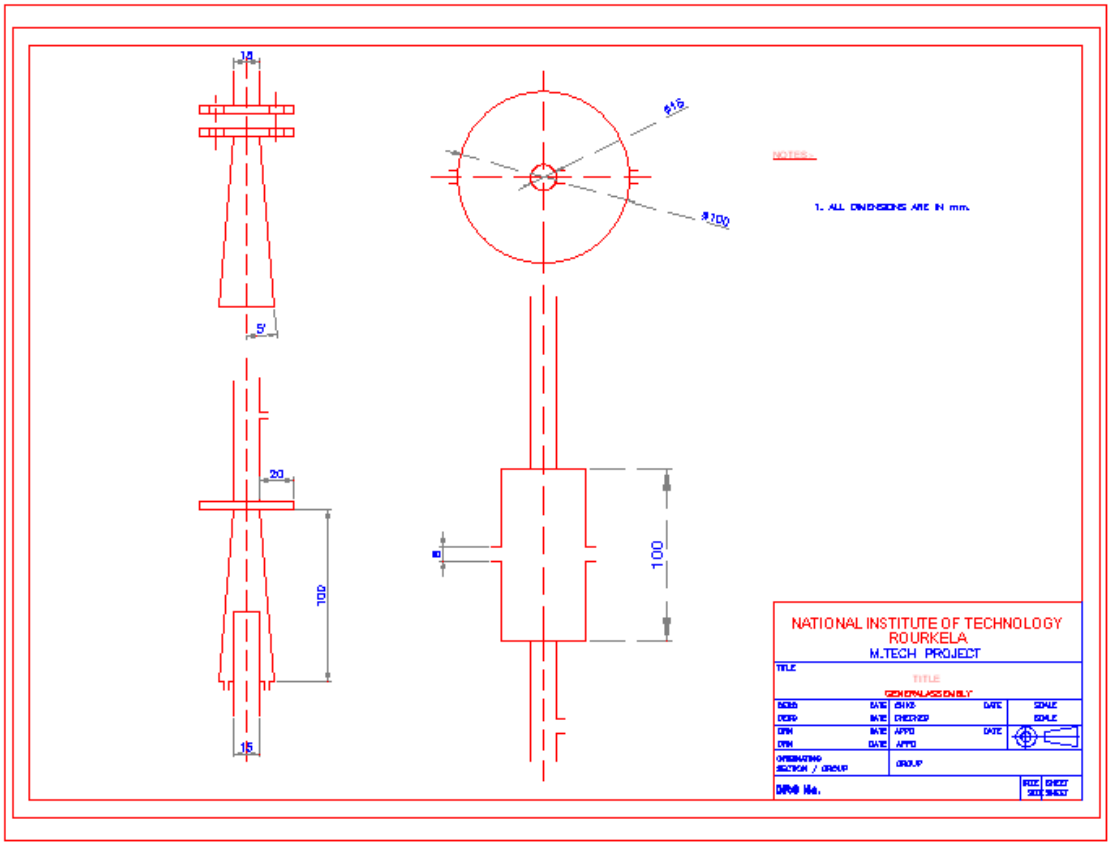

Fig A1- Entry and Exit design for water & air in the set up.

APPENDIX 2

```
%programme to calculate pressure drop in a fuel bundle
clc
close all
Di=138e-3;
Dcr = 38e-3;
D=11.2e-3;
n=54;
rho=1000;
mu=0.001;
v=0:0.01:0.2;
g=9.81;
delz=3.5;
N=6;

A1= pi/4*(Di^2-Dcr^2 - 54*D^2);
De= 4*A1/(pi*(Di + n*D));
Re=rho*v*De/mu;

% Friction factor
for i=1:length(Re)
   if Re(i)<=2300
      f(i) = 64/Re(i);
   else
      f(i) = 0.316/(Re(i)^0.25);
   end
end

figure
plot(Re,f,'');
title('friction factor');
xlabel('Re');
ylabel('f');
grid on;

%   Spacer loss co-efficient
ar = 0.5:0.1:1;
L=15e-3;
D2=3.15e-3;

Re1=input('Enter Renolds no:');
if Re1<=2300
```

```
   f1 = 64/Re1;
else
   f1 = 0.316/(Re1^0.25);
end

Keq = 1./ar.^2 .* (0.5*(1.-ar).^0.75 + f1*L/D2 + (1.-ar).^2);
figure
plot(ar,Keq);

hold on
L=30e-3;
Keq = 1./ar.^2 .* (0.5*(1.-ar).^0.75 + f1*L/D2 + (1.-ar).^2);
plot(ar,Keq,'*-');
hold off;
title('Spacer Loss coefficient');
xlabel('A2/A1');
ylabel('Keq');
legend('L = 15mm','L = 30mm');
grid on;


%   pressure drop
Ar=0.6;
Keq1 = 1/Ar^2 * (0.5*(1-Ar)^0.75 + f1*L/D2 + (1-Ar)^2);
L=15;
delp = 1/2*(f1*L/De + N*Keq1 + (1-Ar)^2)*rho*v.^2 + rho*g*delz;
figure
plot(v,delp);
title('Pressure');
xlabel('velocity');
ylabel('P(bar)');
grid on;
```